Available online at www.sciencedirect.com

ScienceDirect

Geochimica et Cosmochimica Acta 135 (2014) 251–269

Geochimica et Cosmochimica Acta

www.elsevier.com/locate/gca

Lu–Hf isotope systematics of the Hadean–Eoarchean Acasta Gneiss Complex (Northwest Territories, Canada)

Martin Guitreau [a,b,*], Janne Blichert-Toft [a], Stephen J. Mojzsis [a,c,d], Antoine S.G. Roth [e], Bernard Bourdon [a], Nicole L. Cates [c], Wouter Bleeker [f]

[a] *Laboratoire de Géologie de Lyon, Ecole Normale Supérieure de Lyon and Université Claude Bernard Lyon 1, CNRS UMR 5276, 46 Allée d'Italie, 69007 Lyon, France*

[b] *CEPS-Department of Earth Sciences, University of New Hampshire, 56 College Road, Durham, NH 03824-3589, USA*

[c] *Department of Geological Sciences, NASA Lunar Science Institute and Center for Lunar Origin and Evolution (CLOE), University of Colorado, 2200 Colorado Avenue, Boulder, CO 80309-0399, USA*

[d] *Hungarian Academy of Sciences, Institute for Geological and Geochemical Research, 45 Budaörsi ut, H-1112 Budapest, Hungary*

[e] *Institute of Geochemistry and Petrology, ETH Zurich, 8092 Zurich, Switzerland*

[f] *Geological Survey of Canada, 601 Booth Street, Ottawa, Ontario K1A 0E8, Canada*

Received 16 July 2013; accepted in revised form 4 March 2014; available online 8 April 2014

Abstract

The Acasta Gneiss Complex (AGC) is a remnant Hadean–Eoarchean terrane composed of strongly deformed polyphase mafic to felsic gneisses which preserve a multi-stage history of magmatic emplacement, inheritance, and subsequent tectono-thermal modifications. The complexities encountered in such an old terrane fragment have been documented in previous geochronological studies of the AGC (e.g. zircon U–Pb, ^{147}Sm–^{143}Nd), and are evident also in its Lu–Hf isotope systematics. Here, we report new Lu–Hf isotope whole-rock measurements which show that some AGC gneisses were severely disturbed by migmatization and associated mineral segregation, while others preserve their Lu–Hf isotope systematics relatively intact with mostly near- to sub-chondritic initial ^{176}Hf/^{177}Hf ratios. Results reveal identifiable Eoarchean and later (Paleoarchean) magmatic events at around 3960 Ma and again at 3600 Ma, with a major metamorphism of the complex at 3750 Ma. The oldest and least disturbed gneisses have a Lu–Hf regression age of 3946 ± 87 Ma, in good agreement with U–Pb zircon geochronology. A role of yet older crust (4000–4200 Ma) in the formation of the AGC is also evident, but seems not to have influenced to first order the Lu–Hf isotope systematics of the 3960 Ma group. The ca. 3960 Ma group is proposed to be representative of its mantle source based on the absence of correlation between $\varepsilon_{Hf(t)}$ and Ce/Pb. It is further suggested that these two parameters show that the ca. 3600 Ma gneisses were sourced in part from a mafic lithology belonging to the 3960 Ma group, and that multiple sources (mantle and crust) were involved in AGC formation. The identification of preserved Lu–Hf isotope systematics in AGC gneisses means that complementary geochemical and isotopic studies bearing on the petrogenesis of pre-3900 Ma rocks are possible. Despite its history of strong deformation and alteration, carefully selected domains within the AGC carry surviving information about the evolution of the mantle–crust system at the Eoarchean–Hadean boundary.
Published by Elsevier Ltd.

* Corresponding author at: CEPS-Department of Earth Sciences, University of New Hampshire, 56 College Road, Durham, NH 03824-3589, USA. Tel.: +1 603 862 4793.

E-mail address: martin.guitreau@unh.edu (M. Guitreau).

http://dx.doi.org/10.1016/j.gca.2014.03.039
0016-7037/Published by Elsevier Ltd.

1. INTRODUCTION

Unveiling the mechanisms of the emergence of the first felsic crust on Earth, and formulating a means to trace its volumetric extent through time, has far-reaching implications for understanding the thermal budget of our planet (e.g. Jaupart et al., 2007) as well as the co-evolution of the biosphere and geosphere. Concurrent with the different advancements in our perception of the overall physical and chemical evolution of our planet are the various diverse and mutually inconsistent models for crustal growth that have been put forward over the years (e.g. Hurley and Rand, 1969; Fyfe, 1978; Reymer and Schubert, 1984; Taylor and McLennan, 1985; Armstrong, 1991; Belousova et al., 2010). The first-order physical, chemical, and isotopic parameters of Hadean mantle(s) that gave rise to Earth's primordial crust are highly debated (e.g. Boyet and Carlson, 2005; Harrison et al., 2005; Davies, 2007). Nevertheless, progress has been forthcoming recently in elucidating the planet's source composition (e.g. Fitoussi and Bourdon, 2012) and in shedding light on aspects of its early geodynamical regime (e.g. Van Hunen and Moyen, 2012). Direct evidence of formative processes that could be obtained from terrestrial rocks older than 3700 Ma is, however, scarce. The importance of such ancient terrestrial samples lies in the fact that they represent the sole direct testimonies of the first billion years of Earth history against which to test the models cited above and assess their validity.

One such example is the Acasta Gneiss Complex (AGC) in the Northwest Territories of Canada. Based on zircon ion microprobe U–Pb geochronology (Bowring et al., 1989a; Stern and Bleeker, 1998), the AGC hosts the oldest pieces of crust with estimated ages between 3920 and 4030 Ma. Previous studies by Bowring et al. (1989b) reported conventional ^{147}Sm–^{143}Nd isotope analyses that showed these rocks to have CHUR model ages between 3850 and 4100 Ma, broadly consistent with zircon geochronology. Identifying the relationship between a radiometric age and a specific geologic event, such as emplacement of a particular package of crust, is far from straightforward for the Acasta gneisses. Reliable determination of the formation age is complicated by the presence of 4000–4200 Ma xenocrystic zircon cores in some Acasta samples (Iizuka et al., 2006; Guitreau et al., 2012; Mojzsis et al., 2014). The assorted ancient (pre-3960 Ma) ages have two important implications for the history of the AGC: (i) they push the origin of some Acasta protoliths well into the Hadean eon (>3850 Ma), up to about 200 million years earlier than the start of the rock record, and (ii) they open up the possibility that pieces of pre-4000 Ma crust may still be found. Iizuka et al. (2007, 2009) initiated a new era of work on the AGC when they reported on U–Pb geochronology and Lu–Hf isotope systematics of zircons from granitic gneisses collected from a wide area across the AGC, which also resulted in the first detailed geologic map of the region. The Hf isotope compositions of these samples turned out to be complex with negative initial ε_{Hf} values (mean of about −2 at 3960 Ma), which, along with the ca. 4200 Ma xenocryst zircon ages, led Iizuka et al. (2009) to conclude that the AGC protoliths had significantly interacted with older Hadean crust at the time they formed. Bowring and Housh (1995) presaged these results when they used Sm–Nd isotope data to support the argument for a long pre-history of crustal recycling in the AGC. In contrast, Scherer et al. (2010) recorded significantly positive ε_{Hf} values (+6) on whole-rock samples that were used to define an isochron indicating an age of about 4010 ± 60 Ma.

These conflicting results have obfuscated what can be inferred about the chemical and isotopic nature and evolution of the AGC mantle source and the earliest history of the crust. Although negative initial ε_{Hf} values for the AGC could be interpreted as representative of the mantle source prior to 4 billion years ago, no evidence in favor of this hypothesis can be extracted from the accessible rock record. The data available for Acasta rocks point to some degree of crust assimilation, but the actual emplacement ages of the Acasta gneisses have long remained poorly known and hence the meaning of the overall distribution of zircon ages inadequately understood. Recently, however, Mojzsis et al. (2014) reported integrated U–Th–Pb and trace element (Ti, REEs) zircon versus whole-rock data in such a way as to enable the identification of different lithological components of an AGC gneiss collected in the central part of the complex (their sample BNB99-151B; see Section 5.1) and compared these findings to other gneisses from elsewhere in the AGC. Results from that work show that some of the oldest lithologies match the mineral chemistry of zircon populations based on predicted partition coefficients for REE elements between mineral (zircon) and melt (whole-rock compositions). An important outcome was to show that the AGC emplacement age from U–Pb zircon geochronology can be conservatively assigned to 3920 ± 18 Ma, and that the compositions of all older (>3960 Ma) zircons in the Acasta gneisses thus far sampled cannot be reconciled with the composition of the rocks that hosted them. Mojzsis et al. (2014) concluded that all pre-3960 Ma zircons in the AGC were inherited from incompletely assimilated pre-existing crust of probable tonalitic nature.

In this work, we study the same well-characterized samples reported in Mojzsis et al. (2014) for their Lu–Hf isotope systematics and compare them with a wider sample collection from various AGC outcrops. Owing to the fact that most of the Acasta rocks documented for U–Pb zircon geochronology are felsic gneisses with tonalite–trondhjemite–granodiorite (TTG) protoliths – wherein Hf is principally contained in zircon – it becomes possible to determine whether the ancient crust assimilation effect is significant by comparing Lu–Hf isotope systematics between the whole-rocks and their constituent zircons. Consequently, this detailed level of characterization opens the way for Lu–Hf whole-rock isotope compositions to be understood and interpreted more completely in the context of existing U–Pb zircon data and Sm–Nd whole-rock isotope systematics. Together with field observations, whole-rock major and trace element data, and Hf isotopes on Acasta gneisses and zircons pre-characterized for their U–Pb ages, we document the preservation of isotopic signatures within the AGC and interpret these values with the goal of deciphering the early magmatic history of the AGC.

2. GEOLOGICAL BACKGROUND

The Acasta Gneiss Complex outcrops along the Acasta River approximately 300 km north of the town of Yellowknife, Northwest Territories, Canada (as reviewed by Iizuka et al., 2007). These gneisses are exposed in the domal cores of several large basement culminations along the western margin of the Archean Slave craton (Bleeker et al., 2000). They form an integral part of a much larger regional basement complex that underlies much of the central and western parts of this craton termed the Central Slave Basement Complex by Bleeker et al. (1999a,b, 2000); see also Bleeker (2002). The flanks of these domes are outlined by a thin ca. 2800 Ma cover sequence of deformed and metamorphosed (but, importantly, not migmatized) quartzites, banded iron-formations, and metavolcanic rocks. In earlier descriptions of the Acasta gneisses, some of these metasedimentary and metavolcanic rocks, locally tightly infolded, were considered as candidate supracrustal components of the AGC (e.g. Bowring et al., 1990). It has since been recognized that they unconformably overlie the more highly metamorphosed basement gneisses (e.g. Bleeker et al., 2000). All of these basement gneisses, including those of the AGC, are thus older than 2800 Ma, with ages ranging from about 2900 Ma (Mesoarchean) to ca. 4000 Ma (Hadean). As extensive (and ill-defined) outcrops along the Acasta River, they consist of variably migmatized heterogeneous tonalitic gneisses that host cm- to km-scale layers and boudins of more mafic gneiss and leucocratic metagabbro; in general, the gneisses are poly-deformed and poly-metamorphosed with the exception of some rare lower-strain windows.

Archean basement culminations along the western margin of the Slave craton form themselves inliers of Archean rocks within the foreland and eastern internides of the ca. 1800–1900 Ma Wopmay orogen (King, 1986; Hoffman, 1988), a Paleoproterozoic orogen that deformed the western margin of the Slave craton and may have involved the accretion of allochthonous terranes. Basal quartzitic sediments, overlain by metacarbonates and metapelites, representing a ca. 2000 Ma autochthonous cover on the western margin of the craton, were deformed during these Proterozoic collisional processes and locally overlie and dip away from the Acasta gneisses. The Archean basement domes were thus re-deformed and amplified during Paleoproterozoic deformation, with metamorphic grade reaching amphibolite facies. The severity of this ca. 1800–1900 Ma overprint is more intense at higher structural levels, in more highly deformed Paleoproterozoic rocks, than in the basement (e.g. St-Onge and King, 1987).

The antiquity of the Acasta gneisses was discovered in the 1980s, following regional mapping of the Wopmay orogen by the Geological Survey of Canada. Earlier maps depicted the inlier of crystalline rocks along the Acasta River as possible granitoid rocks of the Paleoproterozoic Hepburn Suite intrusives, known from the internides of the Wopmay orogen further north (e.g. Lalonde, 1989). Field observations along the Acasta River, however, showed the rocks to be migmatitic gneisses and thus likely *older* than foliated granitoids of the Hepburn Suite, and likely also older than ca. 2600 Ma granites known from the Slave craton further east. A sample taken during the 1983 field campaign by Janet King (M. St-Onge, pers. comm., 2000) indeed proved to be ancient, with early measurements of zircons pointing to ages as old as 3500 Ma (Bowring and Van Schmus, 1984). Further investigations with the Australian National University's ion microprobe SHRIMP-I of these zircons, as well as zircons from other Acasta samples, yielded an overall age of about 3960 Ma (Bowring et al., 1989a).

In the mid-1990s, the Geological Survey of Canada began a more in-depth study of the age distribution in the AGC in an effort to better understand its chronology and to identify additional rocks from the terrane suitable for further isotopic analyses (e.g. Sm–Nd, Lu–Hf). Up until that time, what had previously been reported was limited to a relatively small number of samples from a restricted area around the original discovery site on an island in the Acasta River (Bowring et al., 1990; Bowring and Housh, 1995). Bleeker and Stern (1997) re-interpreted the formation age of ca. 4017 Ma of the oldest AGC tonalitic gneiss in their new sample collections and presented evidence for several magmatic and metamorphic events subsequent to emplacement of the protolith(s). These events were estimated to have occurred in the Eoarchean at about 3800 and 3740 Ma (both based on zircon cores), in the Paleoarchean to Mesoarchean at about 3630–3618 Ma (based on crystallization of tonalites and gabbros), 3519–3509 Ma (based on zircon cores and metamorphic overgrowths), 3382–3346 (based on overgrowth and granite formation), 3100 (based on evidence for a metamorphic event), and culminating in a Neoarchean event at about 2875 Ma associated with late granite crystallization. It was also noted that the 3382–3346 Ma ages were widespread within the >2700 Ma areas of the Slave craton and corresponded to either a metamorphic or a magmatic event, depending on location. The Neoarchean age is recorded as overgrowths and lower-discordia intercepts (Pb-loss) in zircons from the 4017 Ma tonalitic gneiss cited above, and is interpreted as a high-grade metamorphic event associated with crustal anatexis and large granitic sheet intrusions. Stern and Bleeker (1998) subsequently refined the oldest U–Pb zircon age to 4025 ± 15 Ma.

At about the same time, Moorbath et al. (1997) reported a compilation of Sm–Nd data for a separate collection of Acasta gneisses and used these in conjunction with data from Bowring et al. (1990) and Bowring and Housh (1995) to obtain a whole-rock "isochron" age of 3371 Ma. This age was interpreted by Moorbath et al. (1997) as indicative of a metamorphic event that had so pervasively affected the oldest components of the Slave craton that the Acasta gneisses could not provide useful information about early Earth processes, much less the presence (or absence) of surviving primordial (Hadean) mantle heterogeneities inferred from earlier work.

Work on the AGC resumed in the mid-2000s with investigations of igneous zircons in terms of their coupled U–Pb and Lu–Hf isotope systematics using improved laser-ablation mass spectrometry techniques (Iizuka et al., 2006, 2007, 2009). These detailed studies, along with new field investigations, were used to define four dominant lithotypes in the AGC terrane: (i) a mafic-intermediate series; (ii) a felsic gneiss series; (iii) a layered gneiss series; and (iv) foliated granites. Iizuka and co-authors also reported a major fault (trending NE–SW) that divides the area into a western domain dominated by the "layered gneiss series" and an eastern domain typified by the "felsic gneiss series". The "mafic-intermediate series" rocks in this classification occur as enclaves of plagioclase + hornblende gneisses throughout the eastern domain, whereas they are only present in the western domain as small (<10 m) pods. According to Iizuka et al. (2007), all of these series host 4000 and 3700 Ma ages except for the "foliated granites", which have simple age spectra confined to around 3600 Ma. This level of detailed work has shown that although the field relationships between the four defined lithotypes can be relatively clear at the outcrop scale, the interpretation of age distributions within each of the rock groups is far less obvious.

3. SAMPLE PROTOCOLS

Sampling localities with exact sample locations are shown on the geological map of the known extent of the AGC in Fig. 1.

3.1. Relative ages of different rock samples

The diverse gneisses that comprise the AGC display highly variable states of strain, but in general are strongly

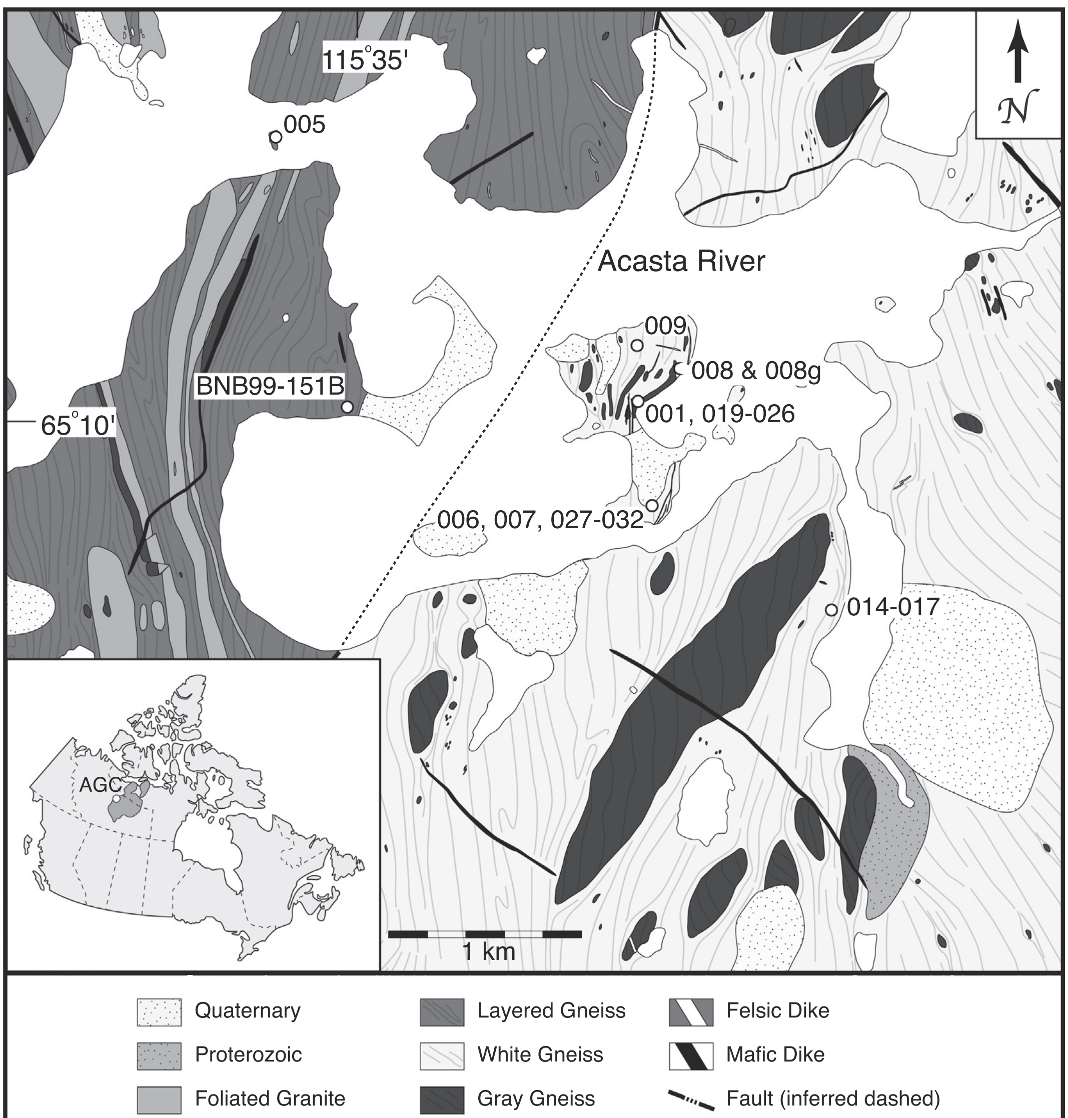

Fig. 1. Geological map of the AGC showing sample locations (after Iizuka et al., 2007 and Mojzsis et al., 2014). The prefix "AG09-" has been removed from sample labeling for easier reading. Note that locations of samples AG09-005, AG09-008, BNB99-151B, and AG09-016 are equivalent to those of SP-405 (Bowring et al., 1989a), BNB95-103 (Bleeker and Stern, 1997), SAB94-134 (Bowring and Williams, 1999), and AC012 (Iizuka et al., 2006, 2009), respectively.

deformed. Complex structures frequently prevent interpretation of spatial relations between various highly deformed mafic and felsic gneissic components. What can be deduced about the relative chronology of the different gneisses in the field – outside of the few outcrops that preserve lower strain – is severely hampered by a complicated deformation history that overprints the whole of the Acasta Gneiss Complex. Overcoming this dilemma requires detailed sampling guided by mapping at the scale adequate to follow field relationships, and sometimes retrospective chronological ordering of components based on the results of radiometric dating. Moreover, the disparate Pb loss patterns and $^{207}Pb/^{206}Pb$ age ranges displayed by most AGC zircons can lead to apparent temporal overlap between different events (e.g. Bowring et al., 1989a; Stern and Bleeker, 1998; Iizuka et al., 2007; Guitreau et al., 2012). This is a serious limitation when attempting to determine accurate ages of different lithologies. Accurate crystallization age determinations of the gneisses are necessary for determining meaningful initial Hf isotope compositions for specific samples but are rendered problematic due to ancient Pb loss effects on $^{207}Pb/^{206}Pb$ ages, even for a <5% discordant zircon (>50 Myr). For example, if a zircon crystallized at 4000 Ma and lost 20% of its Pb at 3600 Ma, at the present day it would show 0.5% discordant U/Pb ages associated with a $^{207}Pb/^{206}Pb$ age of 3937 Ma. This example underscores the challenges faced when seeking accurate crystallization ages for such old rocks. In some cases, ages can even contradict apparent field relationships as discussed in Iizuka et al. (2007). Plagioclase-hornblende ("metagabbro") rocks that comprise the "mafic-intermediate gneiss series" are usually interpreted as the oldest AGC components in most outcrops (Stern and Bleeker, 1998), but these rocks have apparent U–Pb zircon ages that are several hundreds of millions of years younger than the enclosing and cross-cutting granitoid gneisses which host them (Mojzsis et al., 2014). The reason for this is that the melts that gave rise to these rocks had primary igneous compositions that rarely resulted in crystallization of magmatic zircon (Zr < 40 ppm). Later metamorphic zircon growth can, however, occur from breakdown of nominally Zr-containing minerals, hence causing U–Pb zircon age determinations that merely identify the time when metamorphic conditions led to new zircon growth. "Young" zircon ages for such rocks turn out to be irrelevant to both emplacement and crystallization times.

3.2. The Corner outcrop

An embayment on an island within the Acasta River in the central part of the complex (Fig. 1) — site of some of the first geological observations of the area made by King (1986) — hosts several good quality outcrops that encompass many of the key geological features of the AGC. One of these, informally named by the present authors as "the Corner" (Fig. 2a), contains several generations of transposed granitoid intrusions, mafic dikes, and mafic gneiss enclaves (Fig. 2b). The layers have a general

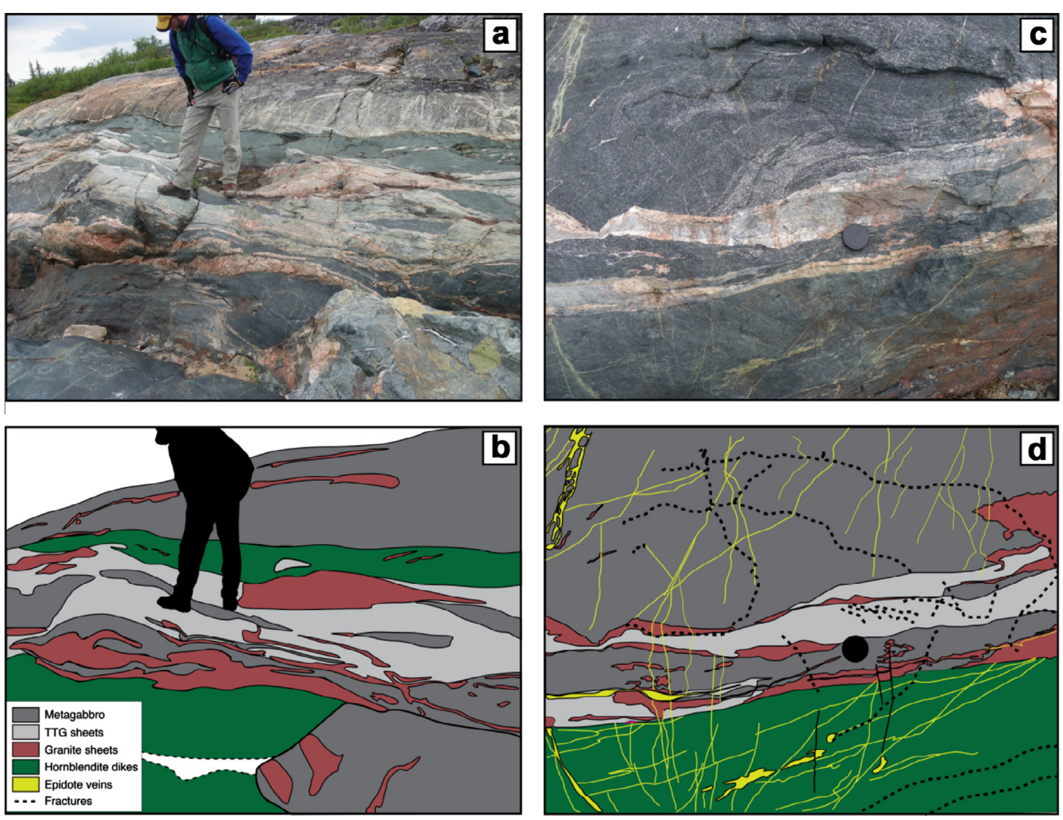

Fig. 2. Northwest-facing view of "the Corner" outcrop (a) with close-up for more detailed unit relationship studies (c) and their respective interpretative sketches (b and d). See text for more details.

northwesterly dip and are composed of a massive but foliated plagioclase + hornblende ("metagabbro") gneiss (AG09-020) that is dark grey to black on fresh surfaces and reddish-brown when weathered. It is intruded by tonalitic to trondhjemitic gneiss sheets (AG09-019, AG09-021-025; light grey in Fig. 2b and d). These two rock types in turn are intruded by younger (lesser- to un-deformed) granites and leucogranitoids (AG09-026), which occasionally occur at the boundary between the purported leucocratic metagabbro and the granitoid gneisses. The youngest recognizable event to affect this outcrop is intrusion by dark green mafic (hornblende-rich) dikes into all other lithologies. In terms of relative proportions of the different lithologies present at this outcrop, the metagabbro makes up roughly 50% by area, whereas the granitoid gneisses, granite, and hornblendite dikes represent, respectively, 15%, 15%, and 20% by area. These field relationships provide a first-order approximation of the chronological sequence of emplacement and later alteration.

Two further volumetrically important lithologies exist on the island outcrops labeled in Fig. 1 (but are not shown in Fig. 2): a massive tonalitic gneiss (AG09-008), which occurs under the last leucogabbroic layer at the base of "the Corner" outcrop, and a granodioritic layer (AG09-009) that sits above another metagabbro body visible at the top of Fig. 2. The massive tonalitic gneiss (AG09-008) presents a conformable transition to sample AG09-008g, which is a less melanocratic garnet-bearing tonalite (Fig. 3a and b). These lithologies have analogs in other locations within the AGC as reviewed by Iizuka et al. (2007).

3.3. Sample description

General descriptions of gneisses encountered in the AGC can be found in Bowring et al. (1989a,b, 1990), Bowring and Williams (1999), Iizuka et al. (2007), Guitreau et al. (2012), and Mojzsis et al. (2014). Detailed petrographic descriptions of rock samples AG09-001, 008, 008g, 009, 014, 015, 016, 017, and 032 are given in the Supplementary material of Guitreau et al. (2012). Sample BNB99-151B ("Slab") components, as well as samples AG09-008, 009, 014, 015, 016, 017, and 020 are described in terms of their petrography and geochemistry in Mojzsis et al. (2014). Based on mineralogy, texture, and crosscutting relationships (see Mojzsis et al., 2014), sample BNB99-151B has been divided into components that belong to five lithologies. The components analyzed here (A, D, F, H, I, K, O, and P) are from lithologies 1 (A, F, and H), 2 (D, I, and K), and 3 (O and P). Lithologies 4 and 5 were not analyzed for Lu–Hf isotope systematics because the former was too small to also be measured for major and trace element concentrations, and the latter, which is a leucocratic vein of trondhjemitic composition, contains abundant inherited zircons from other lithologies, hence providing no unique information about the AGC.

3.3.1. Petrographic characteristics

The Slab (sample BNB99-151B; Fig. 1) is strongly foliated and displays a migmatitic texture overprinted by S-type deformation. The components of this sample essentially display a tonalitic normative mineralogy. Samples AG09-001, 006, 008, 008g, 009, 014-019, 021-025, and 027-032 are all felsic (TTG to granite) gneisses strongly banded and composed of quartz, plagioclase, ± biotite, ± hornblende, and very minor K-feldspar for the major phases. Previously cited ferro-magnesian phases are not always both present in the Acasta gneisses, and biotite is generally the one visible, except in AG09-008, 008g, and 017, where hornblende is abundant (Fig. 3). Two samples contain garnet (AG09-008g and AG09-017) as shown in Fig. 3.

Sample AG09-020, a leucocratic hornblende-plagioclase gneiss corresponding to the massive metagabbro unit in Fig. 2, is composed for the most part of plagioclase and hornblende (Fig. 3e and f). It also has biotite, quartz, and abundant secondary epidote veins.

Samples AG09-007 and 026 are pinkish undeformed late K-rich leucocratic pegmatite and granite (quartz + K-feldspar ± biotite ± muscovite), respectively. These rocks intrude and transect all units to which previously cited samples belong and are equivalent to the pinkish granitic veins visible in Fig. 2.

Samples AG09-019 and AG09-021 to 025 correspond to relatively parallel intrusive tonalitic sheets within the metagabbro (AG09-020) in Fig. 2. In terms of mineralogy they resemble AG09-009, 014, and 015 as described in Guitreau et al. (2012).

3.3.2. Geochemical characteristics

All AGC units analyzed by Mojzsis et al. (2014), except AG09-008, 017, and 020, display typical TTG-like fractionated REE patterns (Fig. 4) and high Sr/Y, high La/Yb, as well as high Na_2O/K_2O. The metagabbro (AG09-020) has a weakly fractionated REE pattern with slight enrichment in light REE, and shows a positive Eu anomaly. We find that this is also the case for all slab components, as well as for a 3962 ± 3 Ma gneiss sample (BGXM) reported in Bowring et al. (1989a), and we interpret this to indicate a cumulative origin. An incomplete published REE pattern for sample BGXM nevertheless matches well that of lithologies 1 (3946 ± 26 Ma) and 2 (3902 ± 4 Ma) reported in Mojzsis et al. (2014). Lithology 3 displays more enriched and less fractionated REE patterns and has been dated at 3881 ± 38 Ma by Mojzsis et al. (2014). Dating of generally xenomorphic zircons, with low Th/U ratios and no clear internal zoning, from samples AG09-020 and 008 by these authors produced very heterogeneous results mostly due to discordance, and indicated poorly defined concordant ages at about 3750–3800 Ma (Mojzsis et al., 2014). A similar observation was made by Guitreau et al. (2012) on samples AG09-008 and AG09-001 estimated at 3750 Ma, which may be a metamorphic age.

3.4. Sample collection and preparation

The sampling strategy for this project employed high-resolution photomapping (1:10 scale) and plane table oriented grid mapping by hand-held GPS and compass of

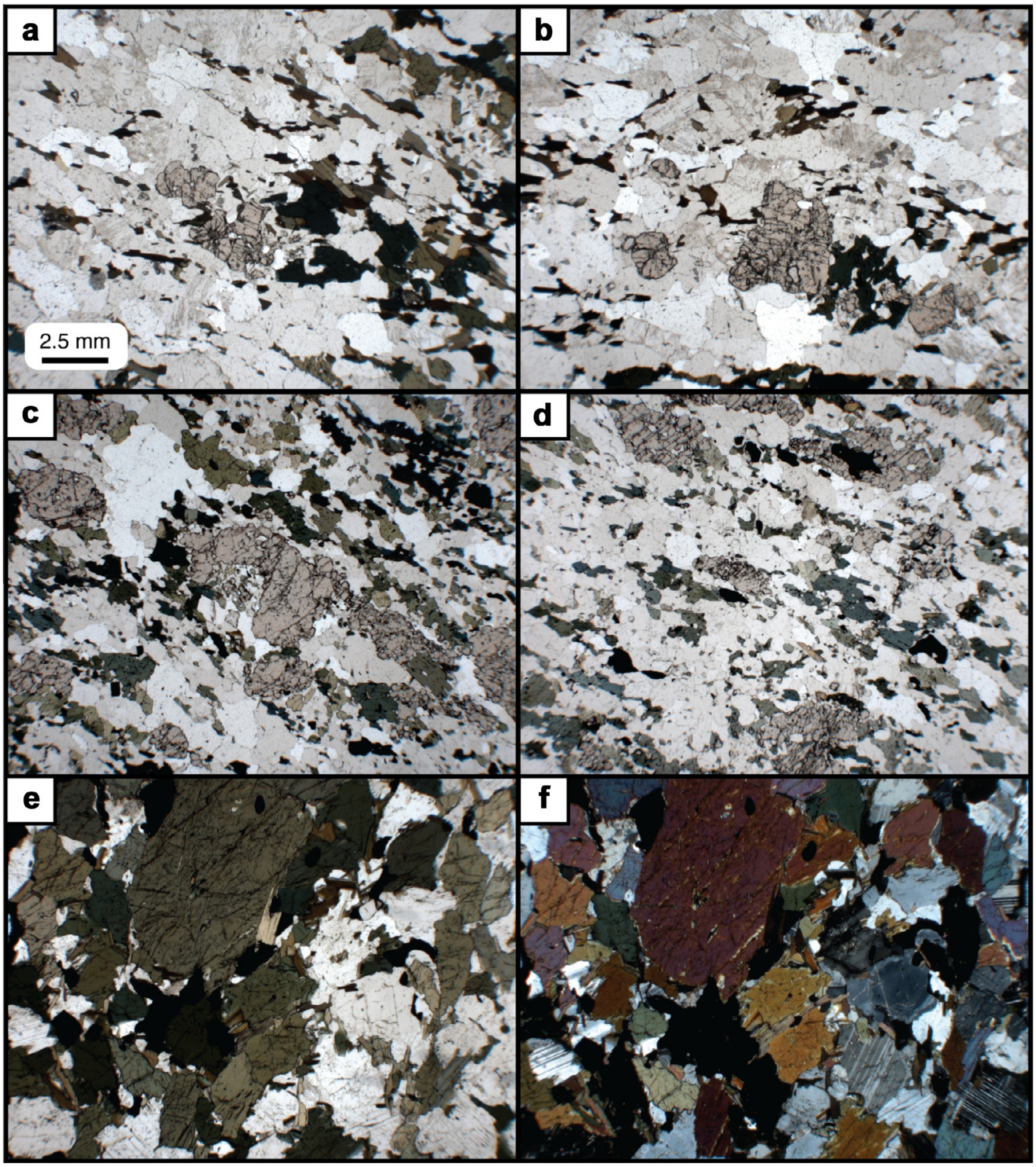

Fig. 3. Thin-section photos of samples AG09-008g (a and b), AG09-017 (c and d), and AG09-020 (e and f) in plane-polarized light except for f, which shows cross-polarized light. Pale pink xenomorphic garnets are conspicuous in both AG09-008g and -017, with higher modal abundance in the latter. The main ferromagnesian phases are biotite in AG09-008g and blue to dark-green hornblende in AG09-017 and AG09-020. In addition to these Fe- and Mg-bearing phases, both samples contain quartz and plagioclase feldspar for the major phases. Both samples have recrystallized metamorphic textures. (For interpretation of the references to colour in this figure legend, the reader is referred to the web version of this article.)

outcrops to comprehensively guide sampling of representative lithologies at each site. Where possible, we directed our sampling priorities to those rocks without secondary veining and away from contacts with other lithologies. This was done with the aim of eliminating potential effects of mechanical mingling or diffusive exchange between unrelated rocks. Any visible secondary veins or weathered surfaces were removed from samples prior to processing, and care was taken to avoid contact with metal tools from the time the sample was collected through to the grinding process. Whole-rock samples were crushed and powdered in either agate mortars at the Laboratoire Magmas et Volcans (Clermont-Ferrand, France), or ceramic mills at the University of Colorado. Thorough cleaning of the pulverizing apparatus with ethanol was done between each sample, and mortar parts were pre-conditioned with small sample aliquots prior to each main sample powdering step.

4. ANALYTICAL TECHNIQUES

4.1. Lu–Hf separation and isotopic analysis

After dissolution of ~250 mg aliquots of whole-rock powder using steel-jacketed Teflon Parr bombs, Lu and Hf

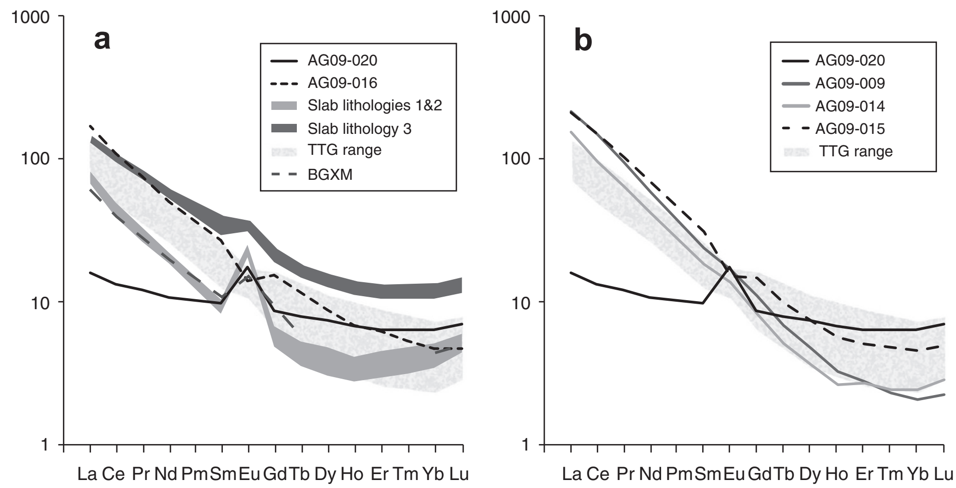

Fig. 4. REE patterns for samples from Mojzsis et al. (2014) and for the Acasta samples analyzed for Lu–Hf isotope systematics in this study and in Guitreau et al. (2012). Patterns for BGMX (Bowring et al., 1990) and the common TTG range (Moyen and Martin, 2012) are shown for comparison. Panel (a) shows samples that are older than 3900 Ma, while panel (b) shows samples that are about 3600 Ma, except for AG09-020, which is shown for comparison.

were separated by ion-exchange column chromatography and measured for their isotopic compositions by MC-ICP-MS (Nu Plasma 500 HR) following the procedures of Blichert-Toft et al. (1997), Blichert-Toft (2001), and Blichert-Toft et al. (2002). Lutetium and Hf concentrations were determined by isotope dilution using a >98% pure mixed ^{176}Lu–^{180}Hf spike added to the samples prior to the digestion procedure and resulted in a precision of 0.2% on the determined ^{176}Lu/^{177}Hf ratios. The JMC-475 Hf standard was analyzed in alternation with the samples, and the mass fractionation-corrected ^{176}Hf/^{177}Hf ratios gave a mean value of 0.282162 ± 0.000012 (2σ, $n = 15$) during the course of the analytical session. This value is identical within error to the accepted value of 0.282163 ± 0.000009 (Blichert-Toft et al., 1997), hence no corrections were applied to the data. Instrumental mass bias was corrected using ^{179}Hf/^{177}Hf = 0.7325 as a reference ratio. Total procedural blanks for Hf and Lu were less than 20 pg. The Lu–Hf isotope results for 26 whole-rock samples and two replicates are listed in Table 1 with ε_{Hf} calculated using the chondritic uniform reservoir (CHUR) values of Bouvier et al. (2008). Initial Hf isotope compositions and ε_{Hf} values for literature data have been re-calculated using this reference frame, even though nearly identical within the quoted error bars to that used in previous studies (Blichert-Toft and Albarède, 1997). The decay constant used in this study for ^{176}Lu is that of Söderlund et al. (2004), slightly improved in precision over the original determination of Scherer et al. (2001). Lu–Hf regression ages together with associated initial Hf isotope compositions were calculated using the ISOPLOT® 3.71 software package of Ludwig (2008).

5. RESULTS

The new Lu–Hf isotope data for the AGC whole-rocks analyzed in this study and described in the following section are listed in Table 1.

Fig. 5 presents the new whole-rock Lu–Hf isotope data in ^{176}Hf/^{177}Hf — ^{176}Lu/^{177}Hf space together with already published whole-rock data from Guitreau et al. (2012), for which corresponding igneous zircons had also been analyzed for their Lu–Hf isotope compositions and dated using the U–Pb chronometer. The data display a broad positive correlation with, for the new data (Table 1), ^{176}Lu/^{177}Hf ranging from 0.00149 to 0.027 and ^{176}Hf/^{177}Hf ranging from 0.280297 to 0.282264 (Table 1), and extending to ^{176}Lu/^{177}Hf and ^{176}Hf/^{177}Hf of, respectively, 0.034 and 0.282653 when adding the data from Guitreau et al. (2012). Two samples, which are a late Archean to Proterozoic pegmatite and K-rich granite, stand out in Fig. 5 by falling above the general trend. For ^{176}Lu/^{177}Hf values below 0.007, the broad positive correlation breaks into two roughly parallel sub-trends (Fig. 5). The upper trend is defined mainly by data for 3600 Ma samples from Guitreau et al. (2012) and tonalitic–trondhjemitic gneiss intrusive sheets from “the Corner” outcrop, which Bleeker and Stern (1997) argued crystallized 3618 ± 21 Ma ago (see Section 3.2; Table 1). The lower trend is defined by data for 3750 and 3960 Ma samples from Guitreau et al. (2012), data for slab components with ages estimated between 3881 and 3942 Ma, as well as new data for undated samples. All data with ^{176}Lu/^{177}Hf above 0.007, with the exception of the late Archean/Proterozoic pegmatite and K-rich granite, correspond to gneisses either dated to be older than 3600 Ma, equivalent to samples for which >3900 Ma igneous zircons have been reported (see Fig. 1), or oldest identifiable components from outcrops (e.g. sample AG09-020; a metagabbro from “the Corner” outcrop). Two slab components (A and D) plot differently than their counterparts with one falling between the two sub-trends and the other plotting away from the positive correlation. Data from Guitreau et al. (2012) show that samples dated at about 3600 Ma have a limited ^{176}Lu/^{177}Hf range, while older samples have a much wider range. When considering

Table 1
Lu–Hf isotope data for samples from the Acasta Gneiss Complex. The letter "r" after some of the sample names indicates replicate analyses.

Sample type	Sample name	Age ± 2σ (Ma)	[Hf] (ppm)	[Lu] (ppm)	$^{176}Lu/^{177}Hf$	2 σ	$^{176}Hf/^{177}Hf$	2 σ	Latitude N	Longitude W
Slab component	A	3942 ± 26	4.17	0.237	0.00805	2	0.281054	3	65°10.058′	115°35.196′
Slab component	D	3902 ± 24	1.92	0.0360	0.00267	1	0.280527	6	65°10.058′	115°35.196′
Slab component	F	3942 ± 26	6.71	0.0800	0.00169	1	0.280347	3	65°10.058′	115°35.196′
Slab component	H	3942 ± 26	9.05	0.125	0.00197	1	0.280344	5	65°10.058′	115°35.196′
Slab component	I	3902 ± 24	12.84	0.131	0.00149	1	0.280336	5	65°10.058′	115°35.196′
Slab component	K	3902 ± 24	11.85	0.125	0.00150	1	0.280297	3	65°10.058′	115°35.196′
Slab component	O	3881 ± 38	12.14	0.258	0.00301	1	0.280444	3	65°10.058′	115°35.196′
Slab component	P	3881 ± 38	16.00	0.449	0.00398	1	0.280404	4	65°10.058′	115°35.196′
TTG	AG-09-005	Unknown	8.05	0.898	0.0158	1	0.281496	3	65°10.865′	115°35.005′
TTG	AG-09-005 r	Unknown	8.02	0.880	0.0156	1	0.281511	4	65°10.865′	115°35.005′
TTG	AG-09-006	Unknown	2.45	0.0773	0.00447	1	0.280596	3	65°09.872′	115°33.640′
Pegmatite	AG-09-007	Unknown	7.05	0.391	0.00787	2	0.281613	3	65°09.872′	115°33.640′
Mafic Tonalite	AG-09-008	3770 ± 31	6.68	0.691	0.0147	1	0.281298	4	65°10.118′	115°33.549′
TTG	AG-09-019	Unknown	4.65	0.082	0.00250	1	0.280549	4	65°10.050′	115°33.803′
Metaggabbro	AG-09-020	Minimum of 3856	0.85	0.161	0.0270	1	0.282264	6	65°10.050′	115°33.803′
TTG	AG-09-021	Unknown	11.40	0.251	0.00312	1	0.280629	3	65°10.050′	115°33.803′
TTG	AG-09-022	Unknown	9.98	0.304	0.00433	1	0.280702	5	65°10.050′	115°33.803′
TTG	AG-09-023	Unknown	9.43	0.269	0.00405	1	0.280681	4	65°10.050′	115°33.803′
TTG	AG-09-024	Unknown	11.37	0.124	0.00155	1	0.280490	4	65°10.050′	115°33.803′
TTG	AG-09-025a	Unknown	11.37	0.177	0.00221	1	0.280551	4	65°10.050′	115°33.803′
TTG	AG-09-025b	Unknown	8.51	0.105	0.00174	1	0.280517	3	65°10.050′	115°33.803′
Coarse grain granite	AG-09-026	Unknown	2.16	0.171	0.0112	1	0.281514	4	65°09.872′	115°33.640′
TTG	AG-09-027	Unknown	2.76	0.0911	0.00468	1	0.280540	4	65°09.872′	115°33.640′
TTG	AG-09-028	unknown	4.25	0.136	0.00453	1	0.280530	3	65°09.872′	115°33.640′
TTG	AG-09-029	Unknown	8.12	0.127	0.00222	1	0.280484	3	65°09.872′	115°33.640′
TTG	AG-09-030	Unknown	3.85	0.0611	0.00226	1	0.280371	3	65°09.872′	115°33.640′
TTG	AG-09-031	Unknown	3.11	0.297	0.0135	1	0.281090	4	65°09.872′	115°33.640′
TTG	AG-09-031 r	Unknown	3.14	0.292	0.0132	1	0.281061	6	65°09.872′	115°33.640′
Data from Guitreau et al. (2012)										
Slab component zircon	2–17	3571 ± 30	179.69	0.565	0.00045	2	0.280407	4		
Slab component zircon	4–10	3700 ± 28	47.40	0.224	0.00067	3	0.280329	10		
Slab component zircon	4–4	3720 ± 16	39.70	0.117	0.00042	2	0.280316	9		
Slab component zircon	2–14	3847 ± 22	284.85	1.111	0.00055	3	0.280167	4		
Slab component zircon	2–15	3850 ± 20	79.26	0.328	0.00059	3	0.280235	4		
Slab component zircon	1–12	3909 ± 24	247.18	0.843	0.00048	2	0.280229	3		
Slab component zircon	3–5	3922 ± 20	39.65	0.105	0.00038	2	0.280250	9		
Slab component zircon	2–3	3993 ± 26	97.34	0.630	0.00092	5	0.280252	6		
Slab component zircon	1–1	4008 ± 20	402.41	1.894	0.00067	3	0.280247	3		

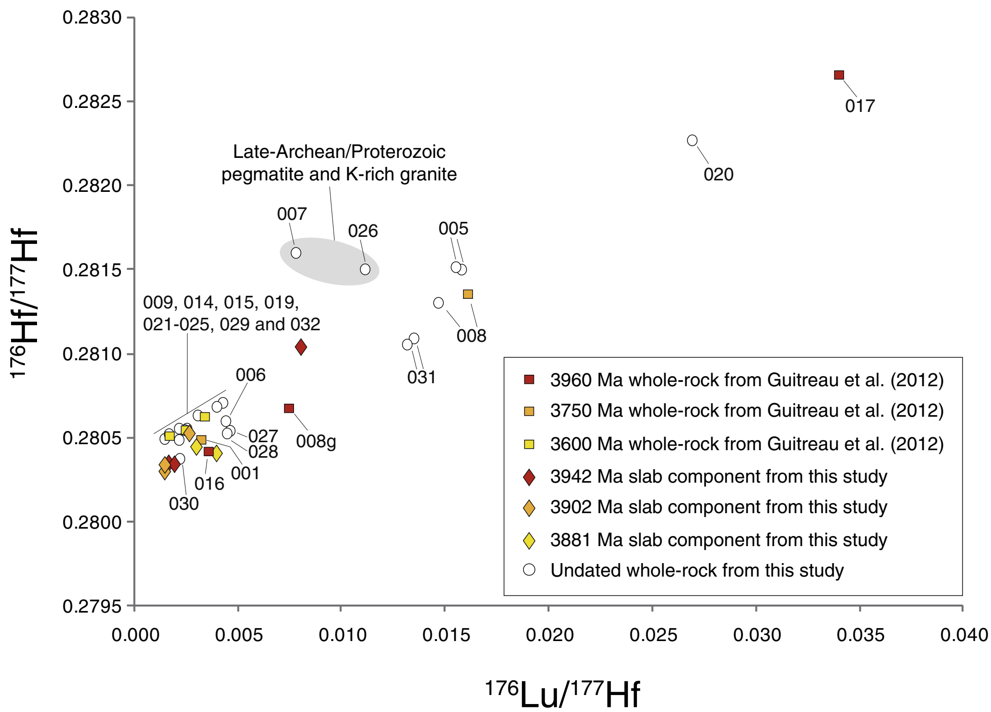

Fig. 5. Whole-rock $^{176}Hf/^{177}Hf$ versus $^{176}Lu/^{177}Hf$ diagram showing the new data from this study together with data for Acasta samples analyzed by Guitreau et al. (2012).

ages expected from field relations for the samples analyzed in this study (see Section 3.2), the new data comply with this behavior, which further matches observations that Iizuka et al.'s (2007) "mafic-intermediate series" is often the oldest identifiable component from available outcrops, while more felsic series seem to be younger.

Lu–Hf isotope data for 3600 Ma samples from Guitreau et al. (2012) yield a least squares regression age of 3530 ± 354 Ma (MSWD = 8.7), while all samples from the upper sub-trend, when excluding sample AG09-029 (which plots slightly below the upper trend), yield an age of 3879 ± 540 Ma (MSWD = 7.8). The same rocks have a least squares regression age of 4017 ± 790 Ma (MSWD = 18) if sample AG09-029 is included. Within the quoted uncertainties both ages are in agreement, but are far too imprecise to be conclusive. However, the initial Hf isotope compositions inferred from the two age estimates cited above are, respectively, 0.280373 ± 31 (2σ) and 0.280361 ± 45 (2σ), hence mutually consistent, and also consistent with the initial $^{176}Hf/^{177}Hf$ of 0.280380 ± 41 (2σ) determined for the 3600 Ma samples from Guitreau et al. (2012) alone. The two samples supposed to be 3750 Ma from U–Pb zircon geochronology (Guitreau et al., 2012) yield a least squares regression age of 3484 ± 58 Ma (initial $^{176}Hf/^{177}Hf$ = 0.280269 ± 6), which is consistent within errors with the age of 3371 ± 59 Ma reported by Moorbath et al. (1997) and interpreted by these authors as a resetting age. All other samples yield a common least squares regression age of 3850 ± 210 Ma associated with an initial $^{176}Hf/^{177}Hf$ of 0.280193 ± 55 (2σ), while gneisses dated at about 3960 Ma by Guitreau et al. (2012) display a consistent, though poorly defined, least squares regression age of 3823 ± 590 Ma (2σ) with an initial $^{176}Hf/^{177}Hf$ of 0.28014 ± 24 (2σ).

6. DISCUSSION

6.1. Preservation of the Lu–Hf isotope systematics in the Acasta gneisses

Actual preservation of radiogenic isotope systems after closure (i.e. rock crystallization) is an important issue to address before trying to interpret Lu–Hf isotope data for such old rocks. This is especially critical for the AGC as Moorbath et al. (1997), and more recently Mojzsis et al. (2014), reported severe disturbance of the Sm–Nd isotope system for AGC gneisses. However, the sensitivity, or resistance, of radiogenic isotope systems to disturbance depends on undergone metamorphic conditions as well as on the mineralogy of the rocks in question so that a particular radiogenic isotope system may be preserved while another has been largely reset. The AGC mostly is constituted of felsic gneisses containing abundant igneous zircons which buffer the Hf isotope budget of their host rocks. Consequently, as zircon is a highly refractory mineral, the Lu–Hf isotope systematics may well be preserved in some AGC gneisses while the Sm–Nd isotope system is disturbed. One way to test this scenario is to compare Lu–Hf isotope data for whole-rocks with those for their corresponding igneous zircons.

6.1.1. Comparison with igneous zircon Hf isotope systematics

Figs. 6 and 7 present whole-rock initial Hf isotope compositions for the oldest identified components (lithologies 1, 2, and 3) documented by U–Pb zircon geochronology in Mojzsis et al. (2014) for Acasta Slab sample BNB99-151B, as well as data from nine single zircons extracted from these same sample components and analyzed by solution MC-ICP-MS in Guitreau et al. (2012). The zircon initial Hf isotope compositions were calculated using the $^{207}Pb/^{206}Pb$ ages measured on the same zircon dissolutions as those yielding the Hf isotope compositions. Laser-ablation zircon Hf isotope data by Iizuka et al. (2009) and solution chemistry zircon Hf isotope data by Amelin et al. (1999, 2000) are also plotted in Fig. 6 for comparison, while in Fig. 7, Hf isotope data from Guitreau et al. (2012) for whole-rocks and their corresponding igneous zircons measured by laser-ablation are shown. Figs. 6 and 7 illustrate the relationship between initial Hf isotope compositions and $^{207}Pb/^{206}Pb$ ages in zircons from different AGC gneisses but also between initial $^{176}Hf/^{177}Hf$ in zircons and their host rock. It is apparent from the data in these figures that not all slab BNB99-151B components have the same initial $^{176}Hf/^{177}Hf$ calculated at the time they formed but that five out of eight of the whole-rock component samples have mutually consistent initial $^{176}Hf/^{177}Hf$, which also are in good agreement with those of their igneous zircons. If dissimilar components are excluded from consideration, the BNB99-151B whole-rock component and zircon data show three main groups according to both Hf isotopes (0.28020, 0.28029, and 0.28038) and $^{207}Pb/^{206}Pb$ ages (3960, 3710, and 3571 Ma). These observations are comparable to those made by Amelin et al. (1999, 2000) and Iizuka et al. (2009). The patterns in Figs. 6 and 7 show that the large age range displayed by zircons from a given sample is due merely to discordance owing to significant ancient Pb loss as described by Zeh et al. (2011) and Guitreau et al. (2012) and characterized by sub-horizontal distributions in the Hf isotope versus age diagram. If only concordant zircons are considered – indicative of the crystallization age of their host rock for which $^{176}Hf/^{177}Hf$ ratios are reported in Fig. 7 – three age groups (3960, 3730, and 3600 Ma) and two clusters of Hf isotope data (~0.28015–0.28020 and 0.28035–0.2804) emerge from the data. Therefore, the different age and Hf isotope clusters identified in the different data sets presented in Figs. 6 and 7 (Amelin et al., 1999, 2000; Iizuka et al., 2009; Guitreau et al., 2012) are consistent even though they are not all found in every study. However, not unlike what is visible from the whole-rock Lu–Hf isotope systematics shown in Fig. 5, two groups seem to dominate: the youngest, which is ca. 3600 Ma and associated with the most radiogenic $^{176}Hf/^{177}Hf$ group, and the oldest, which is >3900 Ma and corresponds to the least radiogenic $^{176}Hf/^{177}Hf$ group. The 3750 Ma group, as mentioned earlier, is statistically far less represented and has $^{176}Hf/^{177}Hf$

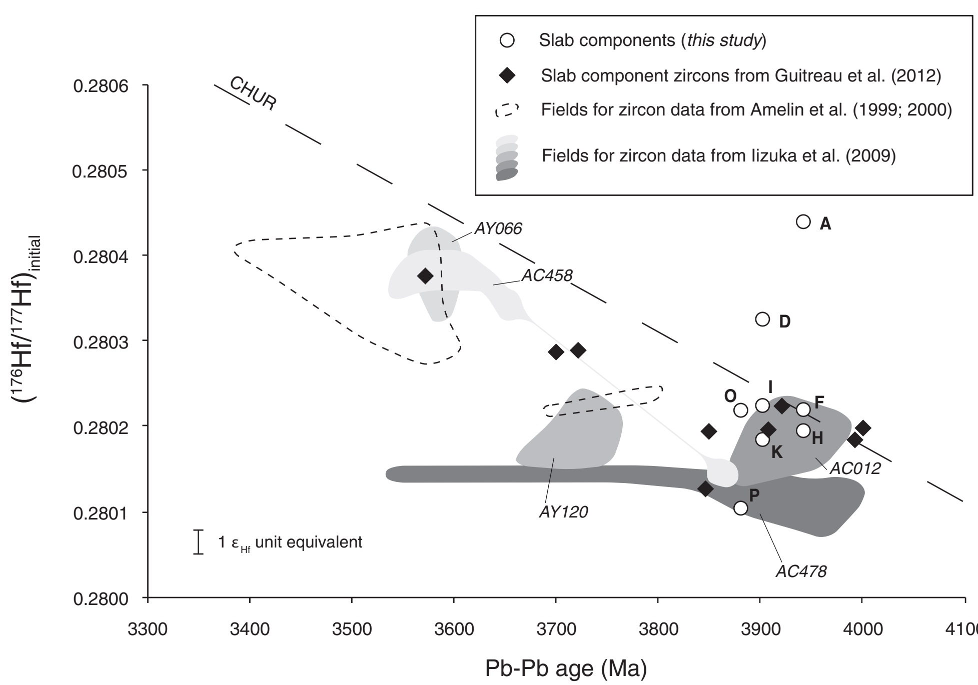

Fig. 6. Initial $^{176}Hf/^{177}Hf$ versus Pb-Pb age diagram with slab component (BNB99-151B) whole-rock measurements compared to previously published zircon solution data from Amelin et al. (1999, 2000) and laser-ablation data from Iizuka et al. (2009). Also reported are solution data from Guitreau et al. (2012) that correspond to zircons extracted from the slab components. Outlined (dashed lines) and shaded grey fields enclose actual zircon data. Samples AY066, AC458, AC012, AY120, and AC478 are from Iizuka et al. (2009) and corresponding zircon fields contain 9, 8, 5, 5, and 18 data points, respectively. Big and small fields from Amelin et al. (1999, 2000) are outlines containing 31 and 2 data points, respectively. Note that sample AC478 from Iizuka et al. (2009) has a zircon population with consistent Hf isotope compositions, while $^{207}Pb/^{206}Pb$ ages vary considerably, which we attribute to ancient Pb loss that affected the zircon crystals to different degrees. Symbol sizes are similar to analytical uncertainties or larger.

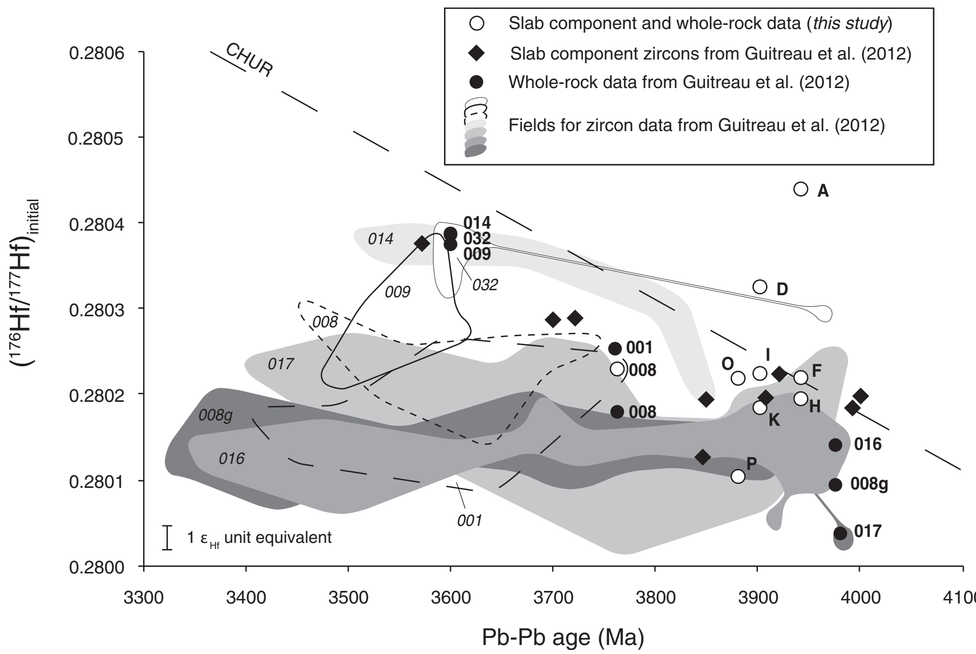

Fig. 7. Initial ^{176}Hf/^{177}Hf versus age diagram showing slab component (BNB99-151B) whole-rock measurements together with Guitreau et al. (2012) slab zircon solution data from Fig. 6. For comparison, whole-rock and corresponding zircon laser-ablation data for eight Acasta samples from Guitreau et al. (2012) are also plotted. The prefix "AG09-" has been removed for clarity. Zircon fields corresponding to samples from Guitreau et al. (2012), which are AG09-001, 008, 008g, 009, 014, 016, 017, and 032, contain 8, 8, 19, 5, 4, 23, 18, and 6 data points, respectively. Note that sample AG09-008 analyzed in this study is a replicate of sample AG09-008 analyzed by Guitreau et al. (2012). Zircons from sample AG09-016 and -008g show the same behavior (between Hf isotopes and ages) as zircons from sample AC478 of Iizuka et al. (2009), indicating ancient Pb loss. Symbol sizes are similar to analytical uncertainties or larger. This figure compares Lu–Hf isotope systematics between zircons and their host rocks and illustrates the relationship between initial ^{176}Hf/^{177}Hf and ^{207}Pb/^{206}Pb ages in zircons showing that when considering the samples with the smallest Pb loss (i.e. most concordant), the initial ^{176}Hf/^{177}Hf of the corresponding AGC rocks was enriched relative to CHUR.

ratios indistinguishable from those of the 3960 Ma group. Fig. 7 further indicates that in most cases initial ^{176}Hf/^{177}Hf ratios displayed by whole-rocks comport well with the initial Hf isotope compositions of their corresponding igneous zircons implying that the Lu–Hf isotope system for these samples evolved in a closed system.

To complement the observations made from Figs. 6 and 7, as well as to more precisely define initial ^{176}Hf/^{177}Hf and ^{207}Pb/^{206}Pb ages for AGC age groups, histograms for igneous zircons are reported in Fig. 8. Fig. 8a shows that the earlier Lu–Hf isotope work reported by Amelin et al. (1999, 2000) did not capture the complete Hf isotope spectrum carried by the AGC rocks (see also Fig. 6) but defines a main peak centered about 0.28039–0.28042. The data set of Iizuka et al. (2009) shows two major peaks for Hf isotopes, with the most radiogenic group corresponding well to the results of Amelin et al. (1999, 2000). The oldest cluster of ages, with Hf isotopes centered about 0.28015–0.28018, matches the peak obtained by Guitreau et al. (2012). Data from the latter study also include a small peak of less radiogenic values interpretable as a result of the presence of inherited old zircon cores (Mojzsis et al., 2014).

The histograms in Fig. 8a underscore the Hf isotope dichotomy that arises from Figs. 5–7. In contrast, the distribution of ^{207}Pb/^{206}Pb ages is far more complex. As for the Hf isotope data of Amelin et al. (1999, 2000), the corresponding Pb isotope data yielded a single well-defined peak, this time corresponding to ages of 3550–3575 Ma. Iizuka et al. (2009) identified other ^{207}Pb/^{206}Pb age peaks with their youngest ages matching those of Amelin et al. (1999, 2000); the other two peaks broadly center about 3750–3775 Ma and 3950–3975 Ma. Data from Guitreau et al. (2012) show an indistinct ^{207}Pb/^{206}Pb age distribution as only one significant peak about 3900–3975 Ma can be confidently identified. A broad peak about 3600 Ma can, however, still be inferred from these data (Fig. 8b); the Pb loss effects seen in Fig. 7 for samples containing zircons older than 3900 Ma are responsible for this broad distribution. When these samples are removed from consideration, a better defined peak centered about 3600 Ma appears. This result is consistent with the reports of Amelin et al. (1999, 2000) and Iizuka et al. (2009) cited above (Fig. 8b). Taken together, the ^{207}Pb/^{206}Pb age distributions, similarly to Hf isotopes, point to a major age dichotomy (at ca. 3600 and ca. 3960 Ma) with a possible weak peak at about 3750 Ma. The age of 3960 Ma was chosen as an average for the oldest samples, despite some small (~1%) differences in their estimated crystallization ages (ranging from ca. 3920 to ca. 3980 Ma; Iizuka et al., 2009; Guitreau et al., 2012; Mojzsis et al., 2014). This is because the range of ages is broadly consistent within uncertainties, and because

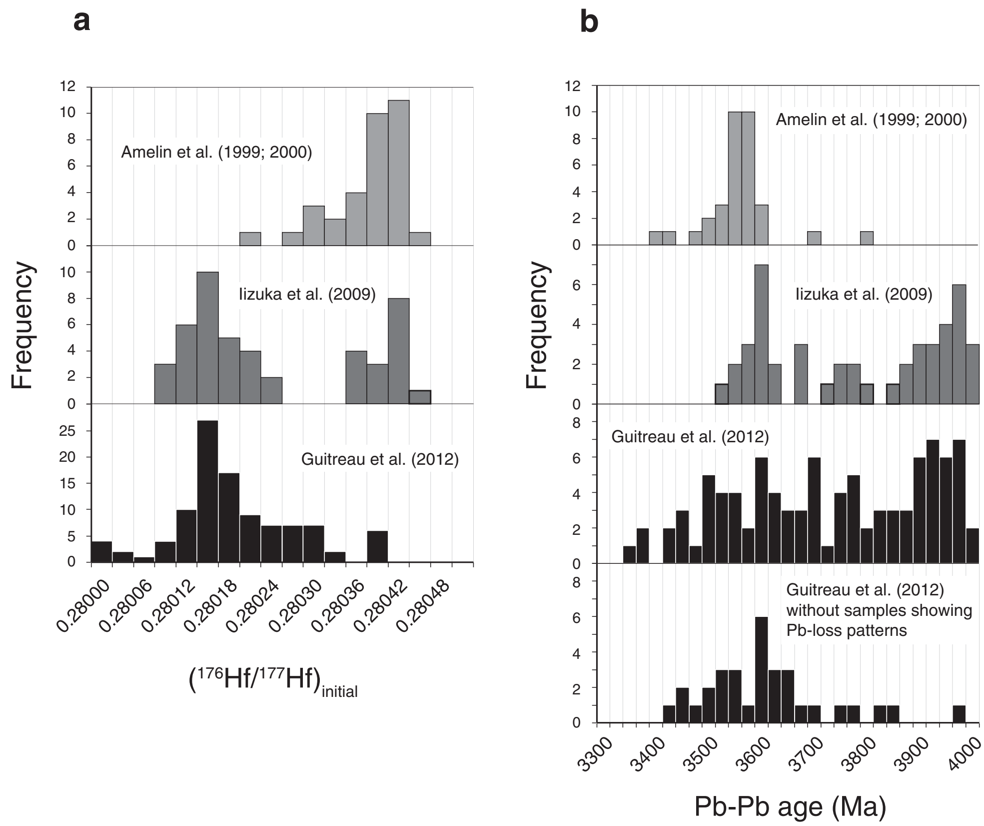

Fig. 8. Histograms showing the distribution of AGC igneous zircon (a) initial $^{176}Hf/^{177}Hf$ and (b) $^{207}Pb/^{206}Pb$ ages for samples analyzed by Amelin et al. (1999, 2000), Iizuka et al. (2009), and Guitreau et al. (2012). These histograms indicate a major dichotomy in the AGC, which is most visible for Hf isotopes as Pb–Pb ages show a large spread (see also Hf isotopes versus age distribution in Figs. 6 and 7). The samples referred to as showing Pb loss patterns in Fig. 6 are AG09-008g, 016, and 017.

zircon ages from these oldest samples show a broad peak in Fig. 8b, indicating a maximum frequency for ages between 3950 and 3975 Ma. This result compares well with the original age estimate of 3962 ± 3 Ma reported by Bowring et al. (1989a). Furthermore, ancient Pb losses that affected these old zircon crystals to different degrees (Bowring et al., 1989a; Stern and Bleeker, 1998; Iizuka et al., 2009; Guitreau et al., 2012; Mojzsis et al., 2014) result in variable apparent present-day $^{207}Pb/^{206}Pb$ ages, even for <5% discordant zircons. Consequently, major and key temporal geological events that correspond well with those defined by Bleeker and Stern (1997) and Iizuka et al. (2007) based on different long-lived radiogenic systems are associated with distinct Hf isotopic signatures (Figs. 6–8) that additionally are in good agreement between different studies (Iizuka et al., 2009; Guitreau et al., 2012).

6.1.2. Comparison with reference isochrons

Ages and initial Hf isotope compositions identified in the previous section can be used as a test for preservation of the Lu–Hf isotope systematics in undated Acasta gneisses analyzed in this study through the construction of three reference isochrons representing the three major events that occurred in the AGC at 3600, 3750, and 3960 Ma. Initial $^{176}Hf/^{177}Hf$ of 0.28039 and 0.28015 attributed to the 3600 and 3960 Ma events, respectively, correspond to the major peaks visible in the histograms in Fig. 8a. The initial $^{176}Hf/^{177}Hf$ for the 3750 Ma group has been determined to be 0.280167, which is the average value derived from zircon data for samples of this age analyzed by both Iizuka et al. (2009) and Guitreau et al. (2012). The 3600 Ma reference isochron fits well the upper sub-trend identified in Fig. 5, which is constituted by an array of gneisses that have ages consistent within analytical uncertainty with that of the reference isochron. The two samples supposed to be 3750 Ma (see Figs. 5 and 7) from U–Pb zircon geochronology show a poor fit to the corresponding reference isochron. Samples identified as the oldest based on U–Pb zircon geochronology and field relationships, globally plot about the 3960 Ma reference isochron (Fig. 9) with a relatively good fit for samples with $^{176}Lu/^{177}Hf$ below 0.01 and sample AG09-020. Two replicates of sample AG09-008, which is supposed to be 3750 Ma, plot closer to the 3960 than the 3750 Ma reference isochron (Fig. 9). The 3960 Ma group is more complicated than the 3600 Ma group (Fig. 9), but its larger range in Lu/Hf should allow for more robust ages to be inferred. One of the only mafic rocks of our AGC sample suite (AG09-020; a metagabbro from “the Corner” outcrop) plots where the 3960 and 3600 Ma isochrons cross, which prevents an age inference to be made for this sample. However, Mojzsis et al. (2014) reported that only metamorphic

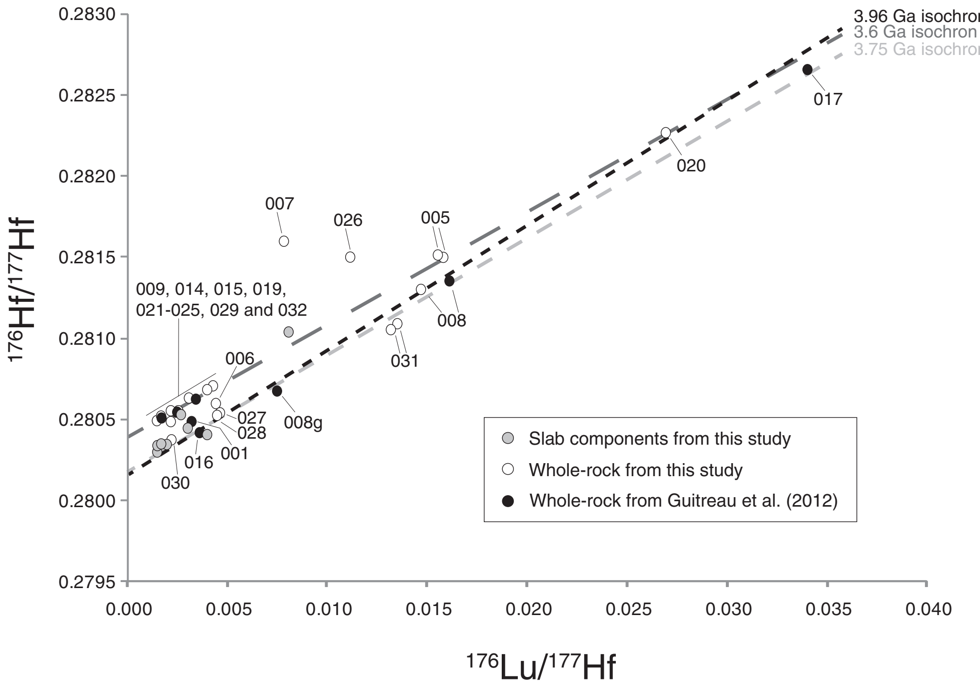

Fig. 9. Whole-rock ^{176}Hf/^{177}Hf versus ^{176}Lu/^{177}Hf diagram showing the same data as in Fig. 5, but here together with reference isochrons constructed using zircon U–Pb ages and corresponding Hf isotope compositions (see Fig. 8).

zircons were recovered from this mafic rock, which indicate ages of ca. 3770 Ga, with the oldest zircon domain being discordant and dated at about 3850 Ma, hence precluding an age of 3600 Ma for this metagabbro. The samples most consistent with the 3960 Ma reference isochron are the main BNB99-151B components as well as samples AG09-030, 027, 028, 020, 008g, and 016, even though the latter two samples have initial Hf isotope compositions different from those of the Slab samples (Fig. 7). Sample AG09-008g, contrary to AG09-016 but similarly to AG09-017, displays lower initial ^{176}Hf/^{177}Hf than its igneous zircons (Fig. 7), hence casting some doubt on the meaningfulness of this value. Therefore, when AG09-008g is excluded, the remaining samples yield a regression age of 3955 ± 120 Ma with an initial ^{176}Hf/^{177}Hf of 0.280193 ± 22 ($\varepsilon_{Hf} = -0.6 \pm 0.8$). When AG09-016 is excluded, the age becomes 3946 ± 87 Ma with an initial ^{176}Hf/^{177}Hf of 0.280200 ± 16, which translates into ε_{Hf} of -0.6 ± 0.6. Consequently, ages determined from whole-rock Lu–Hf isotope systematics are consistent with U–Pb chronology (e.g. Bowring et al., 1989a; Iizuka et al., 2007; Mojzsis et al., 2014), and the initial Hf isotope composition for the 3960 Ma group is well defined and equivalent to -0.2 ± 0.6 epsilon Hf units when calculated at 3960 Ma.

We view the good agreement between reference isochrons and data for some of the AGC samples (Fig. 9) as a key finding. Some Acasta gneisses have kept their Lu–Hf isotope systematics relatively intact since they crystallized and hence significantly raises the importance of the Acasta rocks as valuable archives of the early evolution of Earth's Hadean crust and mantle.

6.2. Disturbance of the Lu–Hf isotope system

Despite overall good preservation of the Lu–Hf isotope systematics in a number of AGC gneisses as discussed in the previous section, a few AGC rocks are not well behaved with respect to their reference isochrons, and otherwise differ from the samples from their presumed age groups, hence preventing straightforward interpretation of their Lu–Hf regression ages and initial Hf isotope compositions. In Fig. 10 is shown how average initial Hf isotope compositions can be determined from each group's regression line. In the same figure, the two garnet-bearing samples (see Fig. 3) show a digression from the 3960 Ma group initial ^{176}Hf/^{177}Hf as Lu concentration increases, which we interpret to arise from overcorrection of radiogenic ^{176}Hf ingrowth. It is important to note that these samples (AG09-008g and 017) have >3900 Ma zircon populations with associated initial ^{176}Hf/^{177}Hf that match other similarly aged populations (Fig. 7). The whole-rock initial ^{176}Hf/^{177}Hf for both samples is not the same as the initial Hf isotopic signature of their corresponding zircon populations, but is significantly less radiogenic at the time these samples formed (Fig. 7).

Garnet has a high partition coefficient for Lu but a low partition coefficient for Hf (Duchêne et al., 1997; Herwartz et al., 2011), such that involvement of this mineral can strongly influence the Lu-Hf isotope system (e.g. Vervoort and Patchett, 1996). Available data for one of the garnet-bearing Acasta samples (AG09-017) show high Y and Yb concentrations (73.5 and 7.67 ppm, respectively) that fall outside the range usually observed for magmatic rocks ($0 < Y < 20$ ppm and $0 < Yb < 2.5$ ppm; data from

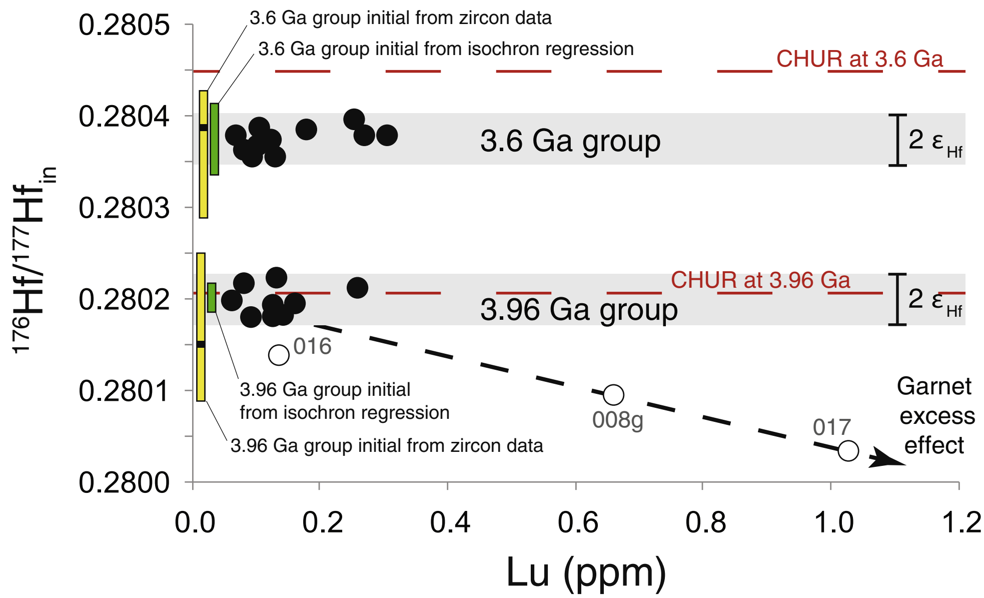

Fig. 10. Initial Hf isotope compositions as a function of Lu concentration of all analyzed Acasta gneisses, showing a clear distribution into two major groups. Also shown are initial $^{176}Hf/^{177}Hf$ estimates for the 3.6 and 3.96 Ga age groups deduced from igneous zircons (see Section 6.1.1) and whole-rock Lu–Hf least squares regressions (see Section 6.1.2). The ranges of variation for igneous zircon initial Hf isotope compositions are shown as well. Black circles correspond to samples identified as undisturbed based on the good match with their respective reference isochrons (see Fig. 9). Open circles are samples dated at ca. 3960 Ma but which have lower initial $^{176}Hf/^{177}Hf$ than samples identified as undisturbed. Samples AG09-008g and -017 are both garnet-bearing and have initial Hf isotope compositions that when calculated at the age indicated by their igneous zircons (ca. 3960 Ma) are lower than those of the zircons (see Fig. 7). The deviation displayed by these garnet-bearing samples from the 3960 Ma group in terms of their initial $^{176}Hf/^{177}Hf$ as Lu increases is interpreted as overabundance of garnet leading to overcorrection of ^{176}Hf ingrowth.

Geochemical Earth Reference Model). Sample AG09-017 contains more garnet than sample AG09-008g (Fig. 3), and hence, Lu whole-rock concentrations correlate with the modal abundance of garnet (Fig. 10). Metamorphic garnets could be responsible for this behavior. The appearance and/or disappearance of metamorphic garnet in a rock should not a priori unbalance the Lu–Hf isotope system as metamorphism alone is an isochemical process. If, however, these gneisses did not behave as a closed system, the presence of excess garnet can result in an overestimation of ^{176}Hf ingrowth; this would mean that garnets were heterogeneously distributed within the gneisses and that the rock samples collected are not representative of their original protoliths. The AGC underwent general migmatization that affected the different generations of gneisses to variable degrees from clearly melted to almost unaffected (Section 2). This partial melting process marks the transition between metamorphism and magmatism leading to significant disturbance of the isotope systems (e.g. Chavagnac et al., 1999, 2001). Complexities observed with AGC whole-rock Lu–Hf isotope systematics are due to generalized migmatization, which at the same time also accounts for the fact that samples containing ca. 3960 Ma zircons align along a 3371 ± 59 Ma Sm–Nd isochron (Mojzsis et al., 2014 and references therein). Samples with higher proportions of leucosomes or melanosomes, which are no longer representative of their magmatic protolith, should plot on internal instead of whole-rock (external) isochrons. Consequently, their present-day Lu–Hf isotope systematics reflect metamorphic/migmatization resetting ages rather than original magmatic protolith ages.

6.3. The Hf isotope composition of AGC source(s) deduced from undisturbed gneisses

As seen in Fig. 10, the initial Hf isotope compositions of the two identified major age groups (3960 and 3600 Ma) can be rather well determined using whole-rock Lu–Hf isotope systematics. This figure also shows the initial $^{176}Hf/^{177}Hf$ determined for each age group using igneous zircon Lu–Hf isotope systematics together with the range displayed by these zircons. Initial $^{176}Hf/^{177}Hf$ estimates are consistent between whole-rocks and zircons for the 3600 Ma group but different for the 3960 Ma group with the initial $^{176}Hf/^{177}Hf$ derived from zircons being lower than that derived from whole-rocks. However, when igneous zircon initial $^{176}Hf/^{177}Hf$ variability is taken into account, initial estimates overlap and zircon data reproduce the whole of the spectrum displayed by whole-rock data. In addition, as also observed in Figs. 6 and 7, the 3960 Ma group probably contains two end-members, represented by AG09-016 for the least radiogenic of them and by the rest of the AGC gneisses for the most radiogenic of them. Therefore, the initial $^{176}Hf/^{177}Hf$ estimate, based on igneous zircons, for this group strongly depends on the actual number of analyzed grains from each sample as this corresponds to a statistical mode. In the present case, the estimate is pulled toward lower initial $^{176}Hf/^{177}Hf$ values

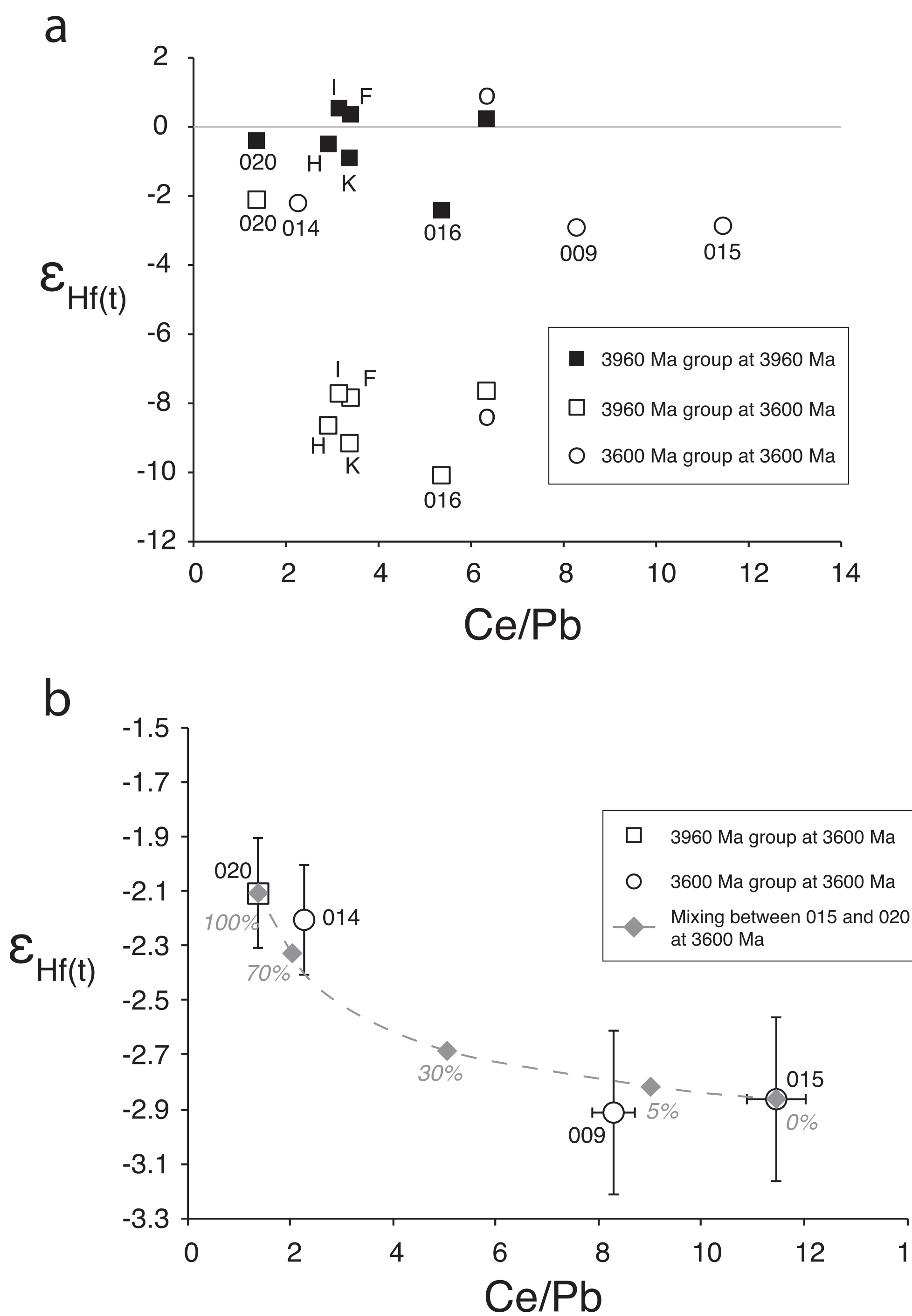

Fig. 11. Epsilon Hf versus Ce/Pb diagrams for Acasta samples analyzed in this study. Diagram (a) shows that no relationship between $\varepsilon_{Hf(t)}$ and Ce/Pb is observed for the 3960 Ma group, which is indicative of limited effects of pre-existing crust contamination on the Lu–Hf isotope systematics of these gneisses. Sample AG09-016, however, may originate from a different source than the rest of this oldest group, giving rise to its apparent discrepancy (see also Fig. 10). In contrast, the 3600 Ma samples display a hyperbolic shape that does not show any relationship with felsic samples from the 3960 Ma group at 3600 Ma, likely indicating the absence of interaction between them. However, sample AG09-020 (metagabbro in Fig. 2) is consistently located on the low-Ce/Pb side of the hyperbola. Diagram (b) is a close-up of (a) for the 3600 Ma samples and AG09-020 at 3600 Ma. Also shown is a calculated mixing curve between AG09-015 and AG09-020, which is consistent with the data. Ce/Pb data are from Mojzsis et al. (2014).

because samples with the highest yield of zircons belong to the least radiogenic end-member, even though the vast majority of analyzed gneisses belong to the most radiogenic end-member. This said, all zircon populations mutually overlap and display a certain variability in initial Hf isotope compositions (Figs. 6 and 7), which is not unexpected for such old and sometimes complex zircons, and can be attributed to the fact that U–Pb age determination and Hf isotope analysis have not been done on the same laser-ablation spots for data published by Iizuka et al. (2009) and Guitreau et al. (2012). In line with this statement, Fisher et al. (2014) have shown that such an approach applied to complex zircons tends to induce higher variability in calculated initial $^{176}Hf/^{177}Hf$, in contrast to concurrent analysis of U–Pb and Hf isotopes. In addition, the presence of ^{176}Yb and ^{176}Lu isobaric interferences on ^{176}Hf in LA-MC-ICP-MS analyses enhances variability in the signal measured on mass 176, resulting in added noise to the measured $^{176}Hf/^{177}Hf$ compared with solution MC-ICP-MS for which Lu and Yb are separated from Hf by ion-exchange chromatography prior to mass spectrometric analysis.

The 3600 Ma gneisses are characterized by subchondritic (negative) initial ε_{Hf} values (ranging from −2.9 to −1.3), while the 3960 Ma group shows negative to near-CHUR values (ranging from −2.4 to +0.6; Section 5). These results point to the involvement of a dominant enriched source in both groups because of the commonly displayed subchondritic initial $^{176}Hf/^{177}Hf$ (Figs. 6, 7 and 10). This source was attributed by Iizuka et al. (2009) to pre-existing crust owing to the fact that evidence for older zircon inheritance and, therefore, crust inheritance in the AGC is indisputable (see also Mojzsis et al., 2014). Most of the samples for which zircons were analyzed show inherited zircons or zircon cores dated at 3700–3800, 3900–4000, 4000–4060, and 4200 Ma (Bleeker and Stern, 1997; Bowring and Williams, 1999; Iizuka et al., 2006, 2007; Guitreau et al., 2012; Mojzsis et al., 2014), which is consistent with interaction with felsic crust. Although inheritance is widespread, it may not have been ubiquitous and thus questions remain concerning its magnitude for both groups. Some samples have preserved their original magmatic Hf isotope compositions as testified to by the reasonably good match between whole-rock initial $^{176}Hf/^{177}Hf$ ratios and those of their igneous zircons (Figs. 7, 9 and 10, Section 6.1). This at least shows that Lu–Hf isotope systematics within these samples have not been significantly disturbed by either post-emplacement metamorphism or crust assimilation, unless igneous zircon crystallization started after significant crust-magma interaction occurred and hence dominated the system.

Two hypotheses can be formulated regarding the interpretation of initial $^{176}Hf/^{177}Hf$ values in the AGC rocks and their actual range. First, we can assume that crust assimilation caused a shift from the original magma Hf isotope composition shared by all rocks from a given age group and hence can explain both initial $^{176}Hf/^{177}Hf$ values and their observed range within this group. Second, despite crust assimilation, primary Hf isotope compositions of some AGC magmas were not significantly modified and hence initial ratios reflect those of multiple sources, including an enriched source (negative initial ε_{Hf}).

Fig. 11a plots the relationship between $\varepsilon_{Hf(t)}$ and available Ce/Pb data as a proxy for crustal contamination (e.g. Jackson et al., 2007). No relationship between the two parameters is observed for the 3960 Ma group indicating that the crust contamination effect on the Lu–Hf isotope systematics was insignificant. This observation suggests very limited allowable interaction of 4200 Ma crust with 3960 Ma magmas, even if it does not exclude such interactions with 4020 Ma crust identified by Mojzsis et al. (2014). The reason for this is that similar initial $^{176}Hf/^{177}Hf$ displayed by the Slab sample (BNB99-151B) and ca. 4000 Ma zircon compared to other >3900 Ma grains (Figs. 6 and 7) prevents 4020 Ma crust assimilation effects on the Hf isotope composition of the 3960 Ma magmas to be detected. The near-chondritic Hf isotope signal carried by the 3960 Ma Acasta gneisses likely is that of their mantle source.

Sample AG09-016 stands out in Fig. 11a, as it does in Fig. 10. Its REE pattern (Fig. 4) is different from those of the other 3960 Ma lithologies and it is the only AGC sample that contains primary muscovite (Guitreau et al., 2012). We therefore postulate that this sample originated from a more evolved source than the rest of the 3960 Ma group. Coupled with its equivalence to Iizuka sample AC012 (to the best of our knowledge) that contains 4200 Ma xenocrystic zircon cores (Iizuka et al., 2006), we hypothesize that this rock is the end result of reworked (pre-existing) continental crust and hence of an ancient enriched source.

Also shown in Fig. 11a are $\varepsilon_{Hf(t)}$ and Ce/Pb data for AGC gneisses that belong to the 3600 Ma group. These define a hyperbola, which on the low-Ce/Pb side is consistent with the Hf isotope signature of sample AG09-020, a metagabbro into which these 3600 Ma gneisses intrude (Fig. 2). Fig. 11b is a close-up of Fig. 11a focusing on the hyperbola displayed by 3600 Ma group gneisses and AG09-020 with ε_{Hf} calculated at 3600 Ma. Mixing lines calculated between AG09-015 and AG09-020 match the observed trend within analytical uncertainty and hence would suggest interaction between these gneisses. Contamination of the 3600 Ma gneisses by AG09-020 is, however, impossible given the amount of contamination required to explain the initial $\varepsilon_{Hf(t)}$ of AG09-014 and the fact that its REE pattern is similar to that of AG09-015 but significantly different from that of AG09-020 (Fig. 4). Rather, this relation may be indicative of involvement (partial melting) of a rock type equivalent to AG09-020 in the petrogenesis of the 3600 Ma gneisses. Another evolved source is needed to explain the $\varepsilon_{Hf(t)}$ versus Ce/Pb relationship for the 3600 Ma group but available data do not allow for its identification.

7. CONCLUSIONS

This work presents new whole-rock Lu–Hf isotope data for 26 samples of the Hadean–Eoarchean Acasta Gneiss Complex. Data reveal the existence of two main Hf isotope signatures that distribute into three age groups that match those previously described for the AGC (Bleeker and Stern, 1997; Iizuka et al., 2007). The age groups are ca. 3600, 3750, and 3960 Ma; the 3600 and 3960 Ma ages are the most commonly represented by far. Remarkably, whole-rock Lu–Hf isotope data for some of the AGC gneisses show good agreement with those of their igneous zircon populations indicating preservation of the Lu–Hf isotope system in the whole-rocks since the crystallization of their protoliths.

The whole-rock data mainly align along two reference isochrons corresponding to ages of 3600 and 3960 Ma. For the 3600 Ma group, the narrow spread in $^{176}Lu/^{177}Hf$ (0.0016–0.0043) combined with the low absolute values result in an imprecise age, while the larger spread for the 3960 Ma group ($^{176}Lu/^{177}Hf = 0.0015–0.027$) results in a robust age of 3946 ± 87 Ma in good agreement with U–Pb chronology (Bowring et al., 1989a; Stern and Bleeker, 1998; Mojzsis et al., 2014). A few samples do not follow these general observations and their Lu–Hf isotope systematics are shown to have been modified after crystallization by migmatization that disturbed modal proportions of minerals (e.g. garnet) through the development of banding.

The undisturbed AGC samples show subchondritic (negative) initial ε_{Hf} values for the 3600 Ma gneisses (−2.9 to −1.3), while the 3960 Ma group show negative to near-CHUR values (−2.4 to +0.6). Keeping in mind that widespread inheritance from pre-existing crust is documented in the AGC (Iizuka et al., 2006, 2007; Mojzsis et al., 2014), the lack of correlation between initial ε_{Hf} and Ce/Pb nevertheless indicates that the primary Hf isotope signal carried by the 3960 Ma group is likely that of its mantle source. This is notably expressed in the metagabbro sample AG09-020. In contrast, ε_{Hf} and Ce/Pb for the 3600 Ma group define a hyperbola that matches calculated mixing lines between the 3960 Ma metagabbro and one of the 3600 Ma samples at 3600 Ma. This finding, together with whole-rock geochemical considerations, indicate derivation of part of the 3600 Ma group from this metagabbro at 3600 Ma.

The uniqueness of the AGC is that it stands as the oldest terrane thus far discovered on Earth, and is the only accessible direct terrestrial rock record from the Hadean–Archean transition. The preservation of Lu–Hf isotope systematics in some AGC domains calls for further work using complementary elemental and isotopic analyses that have the potential to greatly advance our knowledge of the crust–mantle system on early Earth.

ACKNOWLEDGEMENTS

We have benefitted from discussions with O. Abramov, F. Albarède, P. Peng, R. Stern, D. Trail, and O. Van Breemen. We are grateful to K. Mezger, two anonymous reviewers, and A.E.S. Huang for their constructive comments to the manuscript. Mireille Besairie and Hervé Martin are thanked for help at Laboratoire Magmas et Volcans (Clermont-Ferrand, France) and Damien Mollex is thanked for thin section preparations at LGL-TPE (Lyon, France). J.B.T. acknowledges financial support from the French Programme National de Planétologie of the Institut National des Sciences de l'Univers and Centre National d'Etudes Spatiales, and from the French Agence Nationale de la Recherche (grants BEGDy – Birth and Evolution of Terrestrial GeoDynamics and M&Ms – Mantle Melting – Measurements, Models, Mechanisms). S.J.M. and N.L.C. acknowledge support from the NASA Exobiology and Evolutionary Biology Program (Investigating the Hadean Earth), and the NASA Lunar Science Institute (Center for Lunar Origin and Evolution, CLOE). Additional support to S.J.M. came from a Distinguished Visiting Professorship at the Hungarian Academy of Sciences. We are especially grateful for the logistical assistance for work in the Acasta Gneiss Complex provided by the Geological Survey of Canada and the Northwest Territories Geoscience Field Office in Yellowknife.

REFERENCES

Amelin Y., Lee D.-C., Halliday A. N. and Pidgeon R. T. (1999) Nature of the Earth's earliest crust from hafnium isotopes in single detrital zircons. *Nature* **399**, 252–255.

Amelin Y., Lee D. C. and Halliday A. N. (2000) Early-middle archaean crustal evolution deduced from Lu–Hf and U–Pb isotopic studies of single zircon grains. *Geochim. Cosmochim. Acta* **64**, 4205–4225.

Armstrong R. L. (1991) The persistent myth of crustal growth. *Aust. J. Earth Sci.* **38**, 613–630.

Belousova E. A., Kostitsyn Y. A., Griffin W. L., Begg G. C., O'Reilly S. Y. and Pearson N. J. (2010) The growth of the continental crust: constraints from zircon Hf-isotope data. *Lithos* **119**, 457–466.

Bleeker W. (2002) Archaean tectonics: a review, with illustrations from the Slave craton. *Geol. Soc. London Special Pub.* **191**, 151–181.

Bleeker W. and Stern R. (1997) The Acasta gneisses: an imperfect sample of Earth's oldest crust. *Lithoprobe Rep.* **56**, 32–35.

Bleeker W., Ketchum J. W. F., Jackson V. A. and Villeneuve M. E. (1999a) The central Slave basement complex, part I: its structural topology and autochtonous cover. *Can. J. Earth Sci.* **36**, 1083–1109.

Bleeker W., Ketchum J. W. F. and Davis W. J. (1999b) The central Slave basement complex, part II: age and tectonic significance of high-strain zones along the basement-cover contact. *Can. J. Earth Sci.* **36**, 1111–1130.

Bleeker W., Stern R. and Sircombe K. (2000) Why the Slave province, Northwest Territories, got a little bigger. *Geol. Surv. Canada Current Res.* **2000–C2**, 1–9.

Blichert-Toft J. (2001) On the Lu–Hf isotope geochemistry of silicate rocks. *Geostand. Newslett.* **25**, 41–56.

Blichert-Toft J. and Albarède F. (1997) The Lu–Hf isotope geochemistry of chondrites and the evolution of the mantle–crust system. *Earth Planet. Sci. Lett.* **148**, 243–258.

Blichert-Toft J., Chauvel C. and Albarède F. (1997) Separation of Hf and Lu for high-precision isotope analysis of rock samples by magnetic sector-multiple collector ICP-MS. *Contrib. Mineral. Petrol.* **127**, 248–260.

Blichert-Toft J., Boyet M., Télouk P. and Albarède F. (2002) $^{147}Sm–^{143}Nd$ and $^{176}Lu–^{176}Hf$ in eucrites and the differentiation of the HED parent body. *Earth Planet. Sci. Lett.* **204**, 167–181.

Bouvier A., Vervoort J. D. and Patchett P. J. (2008) The Lu–Hf and Sm–Nd isotopic composition of CHUR: constraints from unequilibrated chondrites and implications for the bulk composition of terrestrial planets. *Earth Planet. Sci. Lett.* **273**, 48–57.

Bowring S. A. and Housh T. B. (1995) Earth's early evolution. *Science* **269**, 1535–1540.

Bowring S. A. and Van Schmus W. R. (1984) U–Pb constraints on the evolution of Wopmay orogen, N.W.T. *Geol. Assoc. Can. Prog. Abstracts* **9**, 47.

Bowring S. A. and Williams I. S. (1999) Priscoan (4.00–4.03 Ga) orthogneisses from northwestern Canada. *Contrib. Mineral. Petrol.* **134**, 3–16.

Bowring S. A., Williams I. S. and Compston W. (1989a) 3.96 Ga Gneisses from the slave province, Northwest-Territories, Canada. *Geology* **17**, 971–975.

Bowring S. A., King J. E., Housh T. B., Isachsen C. E. and Podosek F. A. (1989b) Neodymium and lead isotope evidence

for enriched early Archaean crust in North America. *Nature* **340**, 222–225.
Bowring S. A., Housh T. B. and Isachsen C. E. (1990) The Acasta gneisses: remnant of Earth's early crust. In *Origin of the Earth* (eds. H. Newsom and J. Jones). Unversity Press, Oxford, pp. 319–343.
Boyet M. and Carlson R. W. (2005) ^{142}Nd evidence for early (>4.53 Ga) global differentiation of the silicate earth. *Science* **309**, 576–581.
Chavagnac V., Nägler T. F. and Kramers J. D. (1999) Migmatization by metamorphic mineral segregation at subsolidus conditions: implications for Nd–Pb isotope exchange. *Lithos* **46**, 275–298.
Chavagnac V., Kramers J. D., Nägler T. F. and Holzer L. (2001) The behaviour of Nd and Pb isotopes during 2.0 Ga migmatization in paragneisses of the central Zone of the Limpopo Belt (South Africa and Botswana). *Prec. Res.* **112**, 51–86.
Davies G. F. (2007) Dynamics of the Hadean and Archaean mantle. In Earth's oldest rocks. *Dev. Precambrain Geol.* **15**, 61–73.
Duchêne S., Blichert-Toft J., Luais B., Télouk P., Lardeaux J.-M. and Albarède F. (1997) The Lu–Hf dating of garnets and the ages of the Alpine high-pressure metamorphism. *Nature* **387**, 586–589.
Fisher C. M., Vervoort J. D. and Dufrane S. A. (2014) Accurate Hf isotope determinations of complex zircons using the laser ablation split stream method. *Geochem. Geophys. Geosyst.* **15**, 121–139.
Fitoussi C. and Bourdon B. (2012) Silicon isotope evidence against an Enstatite chondrite Earth. *Science* **335**, 1477–1480.
Fyfe W. S. (1978) The evolution of the Earth's crust: modern plate plate tectonics to ancient hot spot tectonics. *Chem. Geol.* **23**, 89–114.
Guitreau M., Blichert-Toft J., Martin H., Mojzsis S. J. and Albarède F. (2012) Hafnium isotope evidence from Archean granitic rocks for deep mantle origin of continental crust. *Earth Planet. Sci. Lett.* **338**, 211–223.
Harrison T. M., Blichert-Toft J., Müller W., Albarede F., Holden P. and Mojzsis S. J. (2005) Heterogeneous Hadean hafnium: evidence of continental crust at 4.4 to 4.5 Ga. *Science* **310**, 1947–1950.
Herwartz D., Nagel T. J., Münker C., Scherer E. E. and Froitzheim N. (2011) Tracing two orogenic cycles in one eclogite sample by Lu–Hf garnet chronometry. *Nat. Geosci.* **4**, 178–183.
Hoffman P. F. (1988) United Plates of America, the birth of a craton: early Proterozoic assembly and Growth of Laurentia. *Ann. Rev. Earth Planet. Sci.* **16**, 543–603.
Hurley P. M. and Rand J. R. (1969) Pre-drift continental nuclei. *Science* **164**, 1229–1242.
Iizuka T., Horie K., Komiya T., Maruyama S., Hirata T., Hidaka H. and Windley B. F. (2006) 4.2 Ga zircon xenocryst in an Acasta gneiss from northwestern Canada: evidence for early continental crust. *Geology* **34**, 245–248.
Iizuka T., Komiya T., Ueno Y., Katayama I., Uehara Y., Maruyama S., Hirata T., Johnson S. P. and Dunkley D. J. (2007) Geology and zircon geochronology of the Acasta Gneiss Complex, northwestern Canada: new constraints on its tectonothermal history. *Precamb. Res.* **153**, 179–208.
Iizuka T., Komiya T., Johnson S. P., Kon Y., Maruyama S. and Hirata T. (2009) Reworking of Hadean crust in the Acasta gneisses, northwestern Canada: evidence from in-situ Lu–Hf isotope analysis of zircon. *Chem. Geol.* **259**, 230–239.
Jackson M. G., Hart S. R., Koppers A. A. P., Staudigel H., Konter J., Blusztajn J., Kurz M. and Russell A. (2007) The return of subducted continental crust in Samoan lavas. *Nature* **448**, 684–687.
Jaupart C., Labrosse S. and Marechal J.-C. (2007) Temperatures, heat and energy in the mantle of the Earth. *Treatise Geophys.* **7**, 253–303.
King J. E. (1986) The metamorphic internal zone of Wopmay orogen (early proterozoic), Canada: 30 km of structural relief in a composite section based on plunge projection. *Tectonics* **5**, 973–994.
Lalonde (1989) Hepburn intrusive suite: peraluminous plutonism within a closing back-arc basin, Wopmay orogen, Canada. *Geology* **17**, 261–264.
Ludwig K. R. (2008) User's manual for Isoplot 3.6, A geochronological toolkit for Microsoft Excel. *Berkeley Geo. Cent. Spec. Pub.* **4**.
Mojzsis S. J., Cates N. L., Caro G., Trail D., Abramov O., Guitreau M., Blichert-Toft J., Hopkins M. D. and Bleeker W. (2014) Component geochronology in the polyphase ca. 3920 Ma Acasta Gneiss. *Geochim. Cosmochim. Acta* **133**, 68–96.
Moorbath S., Whitehouse M. J. and Kamber B. S. (1997) Extreme Nd-isotope heterogeneity in the early Archaean – fact or fiction? Case histories from northern Canada and West Greenland. *Chem. Geol.* **135**, 213–231.
Moyen J. F. and Martin H. (2012) Forty years of TTG research. *Lithos* **148**, 312–336.
Reymer A. and Schubert G. (1984) Phanerozoic addition rates to the contiental crust. *Tectonics* **3**, 63–77.
Scherer E., Münker C. and Mezger K. (2001) Calibration of the Lutetium–Hafnium clock. *Science* **293**, 683–687.
Scherer E., Sprung P., Bleeker W. and Mezger K. (2010) *The Acasta Gneisses Revisited: Evidence for an Early Depleted Mantle*. AGU abstracts, San Francisco.
Söderlund U., Patchett P. J., Vervoort J. D. and Isachsen C. E. (2004) The ^{176}Lu decay constant determined by Lu–Hf and U–Pb isotope systematics of Precambrian mafic intrusions. *Earth Planet. Sci. Lett.* **219**, 311–324.
Stern R. A. and Bleeker W. (1998) Age of the world's oldest rocks refined using Canada's SHRIMP: the Acasta gneiss complex, Northwest Territories, Canada. *Geosci. Can.* **25**, 27–31.
St-Onge M. R. and King J. E. (1987) Thermo-tectonic evolution of a metamorphic internal zone documented by axial projections and petrological P–T paths, Wopmay orogen, northwest Canada. *Geology* **15**, 155–158.
Taylor S. R. and McLennan S. M. (1985) *The Continental Crust: Its Composition and Evolution*. Blackwell Scientific Publications, Oxford.
Van Hunen J. and Moyen J.-F. (2012) Archean subduction: fact or fiction? *Annu. Rev. Earth Planet. Sci.* **40**, 195–219.
Vervoort J. D. and Patchett P. J. (1996) Behavior of hafnium and neodymium isotopes in the crust: constraints from Precambrian crustally derived granites. *Geochim. Cosmochim. Acta* **60**, 3717–3733.
Zeh A., Gerdes A. and Millonig L. (2011) Hafnium isotope record of the Ancient Gneiss Complex, Swaziland, southern Africa: evidence for Archaean crust–mantle formation and crust reworking between 3.66 and 2.73 Ga. *J. Geol. Soc. London* **168**, 953–963.

Associate editor: Shichun Huang